

Polyphonic Pitch Tracking with Deep Layered Learning

Anders Elowsson

KTH Royal Institute of Technology
elov@kth.se

Abstract

This paper presents a polyphonic pitch tracking system able to extract both frame-wise and note-based estimates from audio. The system uses six artificial neural networks in a deep layered learning setup. First, cascading networks are applied to a spectrogram for frame-wise fundamental frequency (f_0) estimation. A sparse receptive field is learned by the first network and then used for weight-sharing throughout the system. The f_0 activations are connected across time to extract pitch ridges. These ridges define a framework, within which subsequent networks perform tone-shift-invariant onset and offset detection. The networks convolve the pitch ridges across time, using as input, e.g., variations of latent representations from the f_0 estimation networks, defined as the “neural flux.” Finally, incorrect tentative notes are removed one by one in an iterative procedure that allows a network to classify notes within an accurate context. The system was evaluated on four public test sets: MAPS, Bach10, TRIOS, and the MIREX Woodwind quintet, and performed state-of-the-art results for all four datasets. It performs well across all subtasks: f_0 , pitched onset, and pitched offset tracking.

Contents

1. Introduction	4
1.1 Fundamental frequency estimation	4
1.2 Note tracking.....	6
1.3 Overview of the article.....	7
2. Datasets and Evaluation methodology	8
2.1 Training Sets	8
2.2 Test Sets.....	10
2.3 Evaluation metrics	10
2.4 Evaluation reliability.....	11
3. Deep layered learning.....	12
4. Method overview.....	14
4.1 Overview.....	14
4.2 Networks.....	16
5. Computing the filtered spectrogram.....	18
5.1 Overview.....	18
5.2 Computing the initial spectrogram.....	19
5.3 Filtering the spectrogram	18
6. Tentogram	21
6.1 Overview.....	21
6.2 Extracting f_0 training examples	22
6.3 Learning the pitch kernel	22
6.4 Bin offset distribution of the learned kernel.....	24
6.5 Tentogram whitening learned from DCT components.....	25
6.6 Run-time	27
7. Pitchogram	27
7.1 Network	28
7.2 Maximized framewise F-measure - F_{frr}	29
7.3 Run-time	29
7.4 Detecting regions in the Pitchogram.....	30
8. Onset detection.....	32
8.1 Neural flux	32
8.2 Spectral flux.....	34

8.3	Pitch flux.....	34
8.4	Additional features.....	34
8.5	Training.....	35
8.6	Peak-picking onsets	35
9.	Offset detection	36
10.	Note classification.....	38
10.1	Input features	38
10.2	Run-time operation	39
10.3	Training.....	39
10.4	Shifting onsets and framewise F-measure - \mathcal{F}_{fr}	40
11.	Regularization and Training performance	40
11.1	Regularization	40
11.2	Training performance.....	42
12.	Evaluation	43
12.1	Main results.....	43
12.2	Comparison overview	43
12.3	Bach10	45
12.4	MAPS.....	46
12.5	TRIOS.....	50
12.6	Woodwind.....	50
12.7	Combined metric.....	51
13.	Conclusions, Discussion, and Future work	52
13.1	Contributions	52
13.2	Performance	54
13.3	Pruning strategies.....	55
13.4	Regularization and training set.....	56
13.5	Deep layered learning	58

1. Introduction

The ability to perceive and separate pitched sounds is an integral ability of human hearing and auditory processing. It enables us to locate and interpret speech in rich acoustical environments and to follow musical voices in polyphonic mixtures. By accomplishing the latter task in a computational model, some of the most fundamental and important properties of music can be extracted. This article presents a novel method for estimating frame-level fundamental frequencies (f_0 s) and transcribing the onsets and offsets of notes in polyphonic music. These tasks are among the most well-studied in the research field of music information retrieval (MIR).

Pitched instruments produce complex tones, generally consisting of periodic waves (partials) at integer multiples. In polyphonic music, many complex tones sound simultaneously. The fact that the f_0 s of most of these tones also are related through simple integer ratios in Western music scales (e.g., 4/3) means that partials of different tones will overlap extensively. The added complexity from other uncertainties, such as the timbre of the performing instruments, audio processing (e.g., equalization), and microphone characteristics (Elowsson & Friberg, 2017b), makes the task of associating an audio time-frame with a correct set of f_0 s very complex. This task is generally referred to as *multiple fundamental frequency estimation*.

Tone starts (onsets) and tone ends (offsets) are important structural elements of music, conveying rhythmical aspects. The most basic parameters when transcribing notes of the music is the onset time and offset time, together with the associated pitch. These parameters are transcribed in the *note tracking* task. During note tracking, the system must try to account for the same uncertainties also present for fundamental frequency estimation. In addition, the envelope and timbre vary considerably at note starts for different instruments, which further complicates the task.

1.1 Fundamental frequency estimation

Fundamental frequency estimation is one of the most studied tasks in MIR. There have been many implementations based on the identification of partial peaks in the spectrogram, early attempts dating back to the 1970s (Goldstein, 1973). Some of these implementations estimate potential f_0 s by the mismatch between identified peaks and predicted harmonics for tentative f_0 s (Maher and Beauchamp, 2013; Duan et al., 2010; Thornburg & Leistikow, 2004; Yeh et al., 2005). The structure of partials is accounted for in various ways, and f_0 s can be estimated in an iterative procedure. One such example is the implementation by Goto (2000), using an expectation-maximization algorithm to track the predominant melody and the bass line. Klapuri (2003) analyzed harmonic relationships, iteratively identifying and then removing predominant f_0 s from the audio mixture under the assumption of spectral smoothness. This methodology was later extended with an auditory model (Klapuri 2008). The smoothness assumption has also been used in other implementations (Pertusa & Iñesta, 2008; Yeh et al., 2005; Emiya et al., 2010; Dressler, 2017). Another direction has been to focus on odd harmonics (Dressler, 2017), which are not overlapped by f_0 s at an octave above. Many of these models have yielded competitive

results at the time of their publication, but to hand-engineer features may be cumbersome, and it is hard to account for all variables that are useful for predicting f_0 s.

Filter models applied in the time-domain were popular for f_0 -estimation in the 1990s. Two examples are the work by Sethares and Staley (1999), and De Cheveigné and Kawahara (1999), that both employed an iterative removal of identified periodicities in the time domain.

Another direction in f_0 -estimation is to decompose spectral frames from a set of basis patterns (a “dictionary”). This can be done by nonnegative matrix factorization (NMF) (Smaragdis & Brown, 2003), which can be extended by enforcing sparseness with regard to the number of basis vectors (Cont, 2006) or the polyphony level. The dictionary can be tuned based on the analyzed audio (O’Hanlon et al., 2016). The decomposition can also be done with prior subspace analysis (PSA), incorporating certain restrictions (FitzGerald et al., 2005), or probabilistic latent component analysis (PLCA), which reframes the decomposition into a probabilistic framework (Benetos et al., 2013; Benetos & Weyde, 2015; Nakamura et al., 2018). In the general case of NMF, the spectral composition of an instrument is encoded with a basis vector for a frame of audio, sometimes for several common instrument groups, and the algorithm finds a combination of these vectors that can reproduce the analyzed spectrum. The methodology has some drawbacks. It is slow for higher resolutions (higher than a semitone), and the spectral vocabulary is often insufficient for encoding the variation in spectral instrument characteristics in music audio recordings. One proposed improvement for the latter challenge is to model the basis vectors on a few adjacent harmonic partials of the analyzed song (Vincent et al., 2010). Furthermore, NMF assumes that a linear combination of the vectors will suffice to recreate the analyzed spectral frame. This assumption does not hold for overlapping partials from several tones, as the magnitude of the combined partial sinusoids will depend on their relative phases. Pesek et al. (2017) used unsupervised learning to learn compositional layers, mapping activations in the highest compositional layer to a frame of f_0 -estimations during run-time.

Supervised learning can be used to infer an intricate mapping between the input and the objective strictly adapted to the task, something that can be hard to achieve with matrix factorization methods or unsupervised learning. The learned weights can be expected to encode the variation of spectral characteristics found in the training set, while also modeling the uncertainty to which these characteristics can be estimated in polyphonic tonal textures of individual tracks. Many of the spectral relationships the system can be expected to utilize are non-linear. Some of these have previously been modeled by creating handmade features. One important example is to be attentive to partial frequencies of a tentative f_0 that do not coincide with partial frequencies of other tentative f_0 s (e.g., Dressler, 2017).

An early machine learning implementation extracted raw spectral magnitudes within around two octaves of each f_0 to build a support vector machine (SVM) model (Poliner & Ellis, 2006), creating a separate SVM for each note pitch (i.e., not pitch invariant). This direction was also used by Nam et al., (2011). Recently, a convolutional neural network (CNN) was proposed for f_0 -estimation, using time, frequency, and a third dimension

consisting of the first five harmonics and a subharmonic (Bittner et al., 2017). On a similar theme, magnitudes of the first partials have been used as basic features to classify frame-level f_0 s (Schramm & Benetos, 2017). A CNN with a processing scheme more similar to that of image classification (local receptive fields, followed by fully connected layers) was proposed by Sigtia et al. (2016). A CNN using kernels with a range of approximately an octave was proposed by Kelz et al., (2016). Another very recent system uses a CNN in combination with a bidirectional long short-term memory (LSTM) network for computing framewise prediction (Hawthorne et al., 2017).

As evident, it is only just recently that depth and weight sharing has been utilized in systems based on machine learning. Pitch-invariant (and relatively deep) processing strategies were, however, developed in hand-engineered methods much earlier.

1.2 Note tracking

Different methodologies for detecting discrete note events have been proposed. Many of these implementations use frame-level predictions of pitch salience as the input, ultimately trying to discretize this information across time into a set of notes with start and end-points. This has been done with, e.g., dynamic Bayesian networks (Raczynski et al., 2010), a hidden Markov model (HMM) (Vincent & Rodet, 2004; Poliner & Ellis, 2006; Nam et al., 2011) coupled with a musicological model (Ryynänen & Klapuri, 2005; Boulanger-Lewandowski et al., 2012). Other musicological models have been proposed by Sigtia et al. (2014), also using a hashed beam search for note tracking (Sigtia et al., 2016).

Frame-level prediction algorithms may sometimes make mistakes for a few local frames due to small random variations in the input data. The reliability can be increased by median filtering across time (O’Hanlon et al., 2016; Su & Yang, 2015), and by removing thresholded f_0 -activations responsible for a note shorter than 30-80 ms (Benetos et al., 2013; Benetos & Weyde, 2013; Benetos & Weyde, 2015; Nakamura et al., 2018).

Onsets

In some implementations, onsets of the notes are extracted separately. An early attempt at using neural networks for onset prediction was proposed by Marolt (2001; 2004). In this system, a separate network is trained for each note pitch (i.e., no weight sharing across pitch), using input from framewise partial tracking networks. The system is named “SONIC,” and is part of the comparison in the evaluation (Section 12). Some systems extract information guided by detected f_0 -activations and apply a classifier with this information as input. Systems may for example extract the estimated note length from frame-level pitch-blocks (Valero-Mas et al., 2016), features capturing the magnitude of the change in pitch activation (Weninger et al., 2013), or features capturing the spectral flux (Valero-Mas et al., 2017) for a log-frequency spectrogram filtered by a morphological dilation. The latter technique is used to account for pitch-shifts and has been described for onset detection as the *harmonic onset* function (Elowsson & Friberg, 2013) or *vibrato suppression* (Böck & Widmer, 2013). The method by Weninger et al. (2013) determines onset times based on the center of consecutive frames classified as onsets.

Cheng et al. (2016) used an attack-decay NMF for transcription of a piano where the envelope spectrum of each piano key was known beforehand. A similar strategy was employed by Gao et al. (2017), using a differential spectrogram coupled with NMF. Other methods have estimated note starts directly, without relying on a framewise estimate. This has been done for piano recordings with an LSTM network (Böck & Schedl, 2012), and cascading classifiers (Boogaart & Lienhart, 2009); but LSTM networks can also be used in conjunction with framewise estimates (Hawthorne et al., 2017).

Offsets

Offset detection is a subject that has received far less attention than onset detection. Although offsets are not as perceptually important as onsets, they do still provide important information about the musical structure. It is not common to perform offset detection explicitly. Instead, offset positions are extracted together with onsets when notes are extracted directly, e.g., from thresholded f_0 -activations with duration restrictions (Benetos et al., 2013; Benetos & Weyde, 2013; Benetos & Weyde, 2015; Nakamura et al., 2018). Dressler (2017) tracks variation in partial magnitudes and detects offsets when the level drops, weighted according to the stability of the level across time. In the same implementation, a rather high-resolution tracking of pitch also enables the algorithm to detect offsets from pitch shifts. The proposed system will use some similar information but make decisions in a machine learning framework. For monophonic transcription, offsets have instead been determined as the time when the sound level of a note falls below a floor shaped by the sound level of an overall phrase (Friberg et al., 2007).

1.3 Overview of the article

This article presents a deep layered learning methodology for polyphonic transcription. A system for polyphonic transcription with a state-of-the-art performance was used in a MIREX-contribution from 2014 (Elowsson & Friberg, 2014), described only in a shorter abstract. This work is an extension and improvement of that algorithm that expands on the methodology. The datasets and evaluation methodology that were used is presented in Section 2. In Section 3, an introduction to the deep layered learning methodology is given, with a motivation for why this strategy is useful for polyphonic pitch tracking. Section 4 gives an extended overview of the methodology, intended to provide sufficient information for understanding how the various modules contribute to the overall objective. The initial spectrogram filtering is described in Section 5. Then, a detailed description of each learning module is made in Sections 6-10. Section 11 expands on how the spectrum of the music excerpts (MEs) was varied randomly for regularization and shows a layered performance analysis for the training set. The evaluation of the method is finally provided for four public datasets in Section 12. Section 13 offers conclusions and a discussion.

2. Datasets and Evaluation methodology

2.1 Training sets

Two datasets for training were generated from MIDI files, using the GeneralUser GS SoundFont¹. All audio files were synthesized with a sampling frequency of 44100 Hz.

When a MIDI note starts, the corresponding audio samples have an attack during which the energy rises. The perceived onset time of the note will depend on the shape and length of that attack. When a MIDI note ends, the corresponding audio samples have a decay during which the energy falls. The perceived offset time of the note will depend on the shape and length of that decay. Therefore, to increase the accuracy of the onset and offset annotations (from a perceptual perspective), the approximate delay between the MIDI onset/offset and the onset/offset as perceived by the author was estimated for each GM instrument of the SoundFont (this was done manually). The annotated onset times were shifted forward in time 0-0.09 s (mean 0.008 s) for plucked and hammered instruments and 0-0.093 s (mean 0.024 s) for sustained instruments, relative to the MIDI onset information. The annotated offset times were shifted forward in time 0-0.6 s (mean 0.10 s) for plucked and hammered instruments and 0-1 s (mean 0.18 s) for sustained instruments.

Each MIDI file was subsequently preprocessed. First, pedaling was removed, instead extending the offsets for notes sustained by the pedal. Annotations for each note were updated by accounting for the delay previously determined for each GM instrument. For sustained instruments, onsets immediately following an offset of the same pitch were detected, and a gap inserted by shortening the first MIDI note. The length of the gap x was adjusted based on the offset delay d of the GM instrument generating the audio according to $x = 0.7d$, restricting x to the range 0.02-0.3 s. This ensured that the second onset was audible. Notes with an offset within 30 ms of the onset time (according to the manual adjustments on the GM instrument playing them) were extended to 30 ms. If this shifted an annotated offset time to happen after the next onset of the same pitch, the note was removed from the MIDI file.

The first dataset, “*Attacked*,” consisted of plucked and hammered instruments. It contains 145 MIDI files of classical music, collected from the Disklavier e-competition². The dataset was initially screened to remove any of the compositions also present in the MAPS and Bach10 datasets used for testing (Section 2.2). No music by Mozart was included in the training set to increase test independence concerning composition style. MIDI files longer than three minutes were split into three-minute excerpts to facilitate a more efficient load balancing during training, resulting in 454 MIDI files. The instrument used to synthesize each MIDI file was selected randomly according to the distribution presented in Table 1.

The second dataset (*Sustained*) consisted of sustained instruments. The dataset was generated from 369 MIDI files of Bach chorales which had previously been derived from

¹ <http://schriancollins.com/generaluser.php>

² <http://www.piano-e-competition.com/>

Instrument	GM	Prob.
Ac. Grand Piano	1	0.095
Bright Ac. Piano	2	0.095
El. Grand Piano	3	0.095
Honky-tonk Piano	4	0.095
Rhodes Piano	5	0.095
El. Piano	6	0.095
Harpichord	7	0.095
Clavinet	8	0.095
Celesta	9	0.023
Vibraphone	12	0.023
Marimba	13	0.023
Ac. Nylon guitar	25	0.035
Ac. Steel guitar	26	0.035
El. Jazz guitar	27	0.033
El. clean guitar	28	0.033
El. Dist. Guitar	31	0.033

Table 1. GM instruments used in the *Attacked* training set for synthetization, and their probability of being used.

MusicXML files created by Margaret Greentree³. Overlapping compositions present in the Bach10 dataset and MAPS dataset were removed. Audio samples from five instrument groups were used to generate the audio files; Organ (GM 17-19, 21-24), Violin (GM 41-45, 47, 49-52), Brass (GM 57-62, 64) Reed (GM 65-72), and Pipe (GM 73, 75-77, 79-80). For each MIDI file, five versions were made, resulting in a total of 1845 MEs. Each version had four voices. The GM instrument for each voice was selected randomly, with the only restriction that each ME should contain four different instrument groups. Furthermore, for each of the five versions, the global tempo was varied by a factor between 0.9-1.15 and the pitch transposed within ± 2 semitones. The onset time of each note was also varied slightly.

The total number of onsets/offsets and the total number of framewise f_0 s of each dataset are presented in Table 2. About 10 % of the generated MEs were selected for the validation set. For training, the datasets were merged into one training and one validation set.

Number of	<i>Attacked</i>	<i>Sustained</i>
Framewise f_0s	1.03×10^8	1.00×10^8
Onsets/offsets	5.89×10^5	4.78×10^5

Table 2. The two datasets consisting of attacked or sustained instruments. The datasets were designed to have roughly the same number of annotations for the tasks.

³ Previously hosted at www.jsbchorales.net

2.2 Test sets

Four test sets were used. The first was the *MAPS* dataset⁴ developed by Emiya et al. (2010), consisting of piano recordings generated from MIDI using seven virtual pianos (software) and two upright Yamaha Disklavier pianos performed live. This dataset consists of 270 MEs, created from 160 classical compositions, by using some of the MEs several times. The second test set was the *Bach10* dataset⁵ (Duan et al., 2010), which consists of four-voiced Bach chorales. Each voice was recorded separately (real instrument performances) with a bassoon, a tenor saxophone, a clarinet, and a violin. The four voices of each track were then merged into a monaural polyphonic ME, without normalizing the loudness of the different voices.

The third set was the *TRIOS* dataset⁶, which consists of five chamber music trio MEs. Each voice was recorded separately (real instrument performances) and the annotations were manually aligned. One of the tracks contains drums. The fourth dataset was just a single track, a *Woodwind* recording of Beethoven's Variations for String Quartet Op.18 No. 5 (Bay et al., 2009). Each of the five voices was recorded separately and then combined in a monaural polyphonic audio file.

2.3 Evaluation metrics

The performance of the system was evaluated considering framewise f_0 -estimation, note tracking (onsets) and offset detection. When computing evaluation metrics, each estimate and annotation was first assigned a true or false label. A maximum deviation of 50 cents (L_p) was allowed for estimates for both framewise estimates and note-based (the estimated note pitch was used for both onsets and offsets). For note transcription, the onsets were allowed a maximum deviation of L_t 50 ms; for offset transcription, $L_t = 100$ ms was used. The order in which estimates are assigned to annotations during evaluation can be relevant during very fast successions of notes, as shown in Figure 1. Unfortunately, this issue is not addressed in the publication detailing MIREX evaluations (Bay et al., 2009), which has served as a blueprint for polyphonic evaluations since 2009.

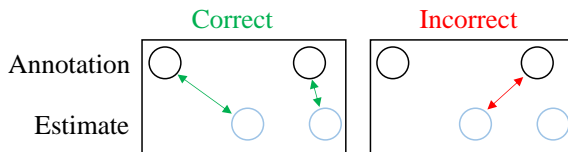


Figure 1. Annotations and estimates correctly paired in sorted order based on distance. When pairing does not happen in sorted order, incorrect pairings may occur.

To avoid unintuitive pairings during fast note succession (or when using longer evaluation windows), estimates were assigned to annotations in order, based on distance.

⁴ <http://www.tsi.telecom-paristech.fr/aao/en/2010/07/08/>

⁵ http://www2.ece.rochester.edu/~zduan/resource/Bach10%20Dataset_v1.0.pdf

⁶ <https://c4dm.eecs.qmul.ac.uk/rdr/handle/123456789/27>

The ordered assignment makes the evaluation more precise, as unintuitive pairings between estimates and annotations are minimized (see Figure 1). The distance d between each estimate and annotation was computed to get a pitch distance (d_p) and, if relevant, a time distance (d_t). A combined distance D was then computed for all estimates within the limits of the pitch, and, if relevant, the time of an annotation. For note detection and offset detection, D was computed as

$$D = 0.85 \left(\frac{|d_t - L_t|}{L_t} \right) + 0.15 \left(\frac{|d_p - L_p|}{L_p} \right). \quad (1)$$

The weights of 0.85 and 0.15 stipulate that proximity in timing is more important than proximity in pitch within the given ranges. For f_0 -estimation, D was computed as

$$D = \frac{|d_p - L_p|}{L_p}. \quad (2)$$

The computations resulted in a sparse 2-dimensional matrix of distances between estimates and annotations. Estimates were paired with annotations in order, starting from the smallest D . Estimates and annotations could only be part of one pair. The number of paired estimates N_{pe} , the total number of estimates N_{te} , and the total number of annotations N_{ta} were used to compute precision \mathcal{P} , and recall \mathcal{R} , as

$$\mathcal{P} = \frac{N_{pe}}{N_{te}}, \quad \mathcal{R} = \frac{N_{pe}}{N_{ta}}. \quad (3)$$

Finally, the F-measure, \mathcal{F} , was computed as

$$\mathcal{F} = 2 \frac{\mathcal{P} \times \mathcal{R}}{\mathcal{P} + \mathcal{R}}. \quad (4)$$

The F-measure will be denoted \mathcal{F}_{fr} for framewise estimates, \mathcal{F}_{on} for onsets, and \mathcal{F}_{off} for offsets. Some previous studies instead use accuracy A , so that was also computed as

$$A = \frac{N_{pe}}{N_{te} + N_{ta} - N_{pe}}. \quad (5)$$

A metric considering both onsets and offsets was also computed using a simpler matching practice, 50 ms for onsets as before, and either 50 ms or 20 % of the note length for offsets – whichever was the largest. As other datasets use “percentages“ instead of fractions, the computed metrics $\times 100$ will be used throughout the article. When not otherwise stated, the datasets were evaluated based on the average performance of all individual notes or framewise f_0 s within the set, and not by averaging over songs or subsets. Arguably, this should give the fairest evaluation.

2.4 Evaluation reliability

When using machine learning or other data-driven methods, it is imperative to perform an unbiased evaluation. If the system has been trained with examples covering a very small subset of timbres present in polyphonic music, and if the test set examples only

cover a similar timbre, the reported \mathcal{F} and A will overestimate the general performance of the system. Unfortunately, it is very common to use biased performance estimates in polyphonic transcription and f_0 -estimation. Many supervised learning systems train and test on recordings from the same instrument or SoundFont. A majority of the NMF-style implementations train and test with the same instruments, several using isolated samples from the test instrument as basis vectors.

The proposed system uses a wide variety of instrument timbres for training (54 different GM instruments) and no overlapping compositions. The four-voiced Bach chorales and compositions for classical piano in the training set, however, have a musical similarity to test sets (Bach10 and MAPS). The evaluation will therefore be especially unbiased for the Woodwind and TRIOS dataset. However, given how common piano music is, it seems reasonable to include such music in any training set as long as no compositions or instruments from the test set are included. Given the wide variety of timbre in the training set, performance should hopefully be more unbiased than many other publications for all four datasets. Systems published before the development of the test sets (i.e., around 2009 or earlier) should however, arguably be the most fairly evaluated.

3. Deep layered learning

The system presented in this article uses a layer-wise combination of *representation learning* and *transfer learning* in a framework which will be referred to as *deep layered learning* (DLL). This framework consists of multiple neural networks, trained individually with supervised learning, but combined to achieve several overall objectives. Layered learning strategies have been employed for e.g. beat tracking (Elowsson, 2016) and polyphonic transcription (Marolt, 2001) in the past. In the proposed system, representations extracted from a filtered time-frequency spectrum are part of the input for all supervised learning steps. Furthermore, the output of a learning layers is passed to classifiers several layers above. The presented framework uses several concepts of DLL, reviewed in the context of MIR by Elowsson (2018):

Learning modules – Each learning step can be understood as a learning module, which infers higher-level representations related to the overarching task. By this definition, the proposed system consists of six learning modules.

Validity - Previous research has suggested that some shallow MIR systems for deep tasks rely on “irrelevant confounding factors” for classification (Sturm, 2013). For highly complex tasks, some important intermediate representations of the input data may be known beforehand. The validity of the system can be enforced by learning these representations in an intermediate step, with the hope of improving generalization capabilities. The assumption is that the system may otherwise be more likely to infer relationships between the input and final targets tuned to the specific characteristics of the training set (see Section 13.5 for an extended discussion). A parallel can be drawn to how weight-sharing mechanisms in CNNs are created to enforce perceptual validity within gradient descent. The proposed system uses the basic assumption that note tracking is best performed on

top of well refined framewise f_0 -estimates. If no f_0 s can be determined, no onsets will be estimated.

Disentangled structures – By accounting for music invariances in MIR systems, generalization and performance can be improved. For example, the log-frequency spectrum of tones, as opposed to the linear frequency spectrum, is to a rather large extent shift-invariant with regard to pitch. This means that weights can be shared across pitch during processing. Certain invariant properties of music may be hard to encode within an end-to-end learning system. By layering the learning steps, and extracting musical structures in mid-level modules, these invariances may sometimes be much easier to account for. The proposed system tracks onsets and offsets for a tone across time along detected f_0 -ridges, which are allowed to vary in pitch (during, e.g., vibrato). Responsible networks can thereby focus on relevant variations in timbre or partial sound levels without being affected by pitch shifts of a tone – they become tone-shift-invariant. Furthermore, the note attack (onsets), the sustained part, and the decay (offsets) are treated as separate features of each note, independent of note length (or pitch). Thereby it becomes possible to represent the note as a vector of fixed size.

Latent representations – When making predictions using multiple layers of connected neurons, the last hidden layer will generally activate for various high-level features, useful for predicting the objective function. These *latent representations* of the input data can be used for tasks not directly trained for. Such a methodology is common in image recognition, e.g., using the last hidden layer of the “AlexNet” (Krizhevsky et al., 2012) for face emotion recognition (Ng et al., 2015). The knowledge acquired for one task is *transferred* to another task (Pan & Yang, 2010). In the proposed system, latent representations of the previous learning modules are used as input for the subsequent learning modules. In a network that predicts f_0 s, some hidden neurons may capture octave relationships, while others react to the level of the 4th and 5th harmonic, etc. As these may influence the prediction of note starts in the subsequent layers in different ways, they could all be used as input for prediction. Therefore, all but the first network use such representations.

Skip connections – Skip connections were first introduced to feedforward networks (Kalman & Kwasny, 1997), and have lately been proposed for deep learning with CNNs (He et al., 2016; Srivastava et al., 2015). In the proposed system, skip connections are used a little differently - latent representations of earlier modules or the spectrogram data are fed to the input of later modules. There is therefore no gradient flowing through them during training. The skip connections are very useful, as intermediate supervised learning steps may not capture all information relevant to the overall objective while making predictions. Although the presence of a f_0 is indicative of an onset, so are variations in timbre - with higher frequencies at note starts. As timbre variations during the tone envelope may be suppressed in higher layers of networks detecting f_0 s, raw spectrogram information is also provided to the networks detecting onsets and offsets.

Pruning – By using cascading classifiers (Alpaydin & Kaynak, 1998; Boogaart & Lienhart, 2009), small classifiers can prune the search space to reject examples that are

certain to be false. In the presented system, the search space for f_0 s is pruned by the first network, and then further reduced in the second bigger network. The resulting speedup enables the model to predict f_0 s at a resolution of centitones rather than semitones. The pruned search space is then the basis for onset and offset detection. A key objective during pruning, as will be shown, is to retain a high recall.

Layered performance supervision – By evaluating aspects relevant to the final objective at each step of the DLL, it becomes possible to find and improve processing steps that limit performance; and to tune the balance between false positive and false negative classifications (affecting recall and precision). The proposed system computes performance measures for all main targets (f_0 s, onsets, and offsets) after each learning step. This is presented for the training set in Section 11.2).

4. Method overview

An overview of the system is provided in this Section, and a detailed description of spectrogram filtering and each learning module is provided in Sections 5-10. The principles for DLL outlined in Section 3 were used to determine the overall architecture. The search space was pruned by discarding the majority of possible pitches and the majority of possible onset positions at an early stage. This results in a relatively fast execution time given the high resolution. Each learning module was designed to infer a non-linear mapping from a lower-level pitch representation (or a latent representation thereof) to a higher-level pitch representation.

4.1 Overview

Figure 2 shows a flowchart of the system. It was trained with the training set described in Section 2.1. The system contains six neural networks (blue arrows in the figure), each one using representations (green boxes) computed in earlier networks. The first layer in each network behaves as a sparse convolutional filter, accomplished by “slicing” the input representations across pitch and, at later layers, time. Between each network, the output activations are processed (yellow boxes) to prepare the system for the next stage in the processing chain. Finally, the output estimates are produced (red boxes). The networks of the system were trained in an iterative fashion, (1) processing the training tracks up until a new network to compute its input, (2) training the network, (3) processing the training tracks with the newly trained network, (4) taking the output from the network and processing the tracks further to prepare the input of the next network, etc. References to Figure 2 are indicated in *italics* in the overview provided below.

First, the variable-Q transform (*VQT*) was computed for each audio file, producing a spectrogram with spectral bins at a log-frequency distribution. The output of the VQT was filtered by applying a noise floor that whitens the spectrum and ensures signal level invariance, resulting in the spectrogram L . The first network then computed tentative framewise f_0 -estimates from a linear combination (N_1) of 50 spectral bins from L . The best performing combinations of spectral bins were selected by iteratively adding bins in

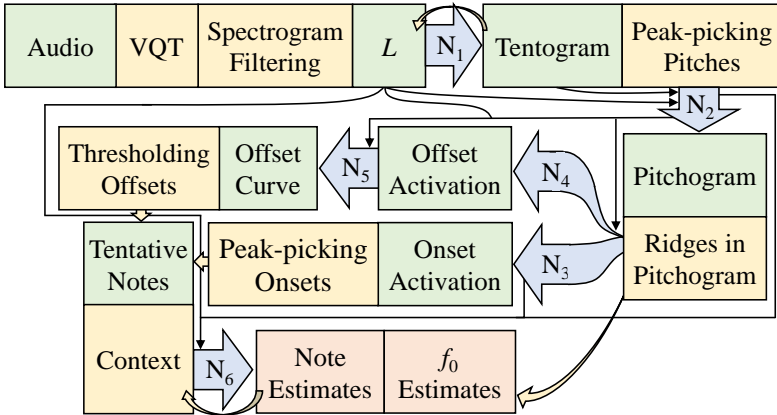


Figure 2. Overview of the polyphonic pitch tracking system. Representations (green), intermediate processing steps (yellow), and the six neural networks (blue arrows – N_1 - N_6) in the DLL architecture that outputs note and f_0 estimates. Representations (including latent such) passed from one network to the input of another (“skip-connections”) are indicated by black arrows.

a forward selection. The 50 bins can therefore be conceived as a *sparse learned kernel*. Prominent tentative f_0 -activations were extracted with *peak-picking* from the *Tentogram* – the output from the linear combination of spectral bins across all pitches. The extracted estimates were updated by performing a more accurate estimation with a bigger (non-linear) network (N_2), resulting in a *Pitchogram*. The Pitchogram can therefore be understood as a more accurate version of the Tentogram, capturing f_0 s across time and frequency. The N_2 network applied the previously computed sparse kernel over both the max-pooled and original spectrum, and also included the activation of other simultaneous tentative pitch activations. As tones are played, f_0 -activations form regions in the Pitchogram, expanding over time. These regions were extracted, and a pitch *ridge* computed for each region.

The activations of the last hidden layer in the Pitchogram network (N_2) are latent representations corresponding to important aspects with relevance to the pitch percept. The variation of these activations (referred to as the neural flux), as well as other relevant spectral features and output activations of N_2 , were extracted along the pitch ridge. They were then used as input to a network (N_3) computing an *onset activation* curve for each region. The spectral input features of each tone thereby become invariant in relation to pitch variations across time, which is useful during vibrato or when the pitch changes rapidly at note starts. After smoothing the onset activation, tentative onsets were extracted by *peak-picking*, with the timing refined by parabolic interpolation. The same input was then used to compute an *offset activation* curve with a fourth network (N_4), from which the final offset position was determined by a fifth network (N_5). After processing all regions, onsets and offsets for a set of *tentative notes* of the ME had thus been established.

Finally, each of these notes was evaluated in the note network (N_6), using previously computed representations as well as information about neighboring notes (pitch and time)

to compute the probability that a note is correct. Incorrect tentative notes were removed one by one for the ME, starting with the tentative notes that are most likely to be incorrect. After removing a note, other notes in the vicinity have their probability updated by the network. With this procedure, tentative notes that are borderline cases are evaluated with a more refined *context*. The remaining notes correspond to the *note estimates*, and the pitch ridge between onsets and offsets of these notes were used as *f₀ estimates*.

4.2 Networks

Table 3 shows an overview of the networks in the system. The networks used the filtered spectrogram (L) together with information from earlier networks to achieve their respective objective. The networks that feed their hidden layers as representations to later networks had two hidden layers. The size of the first hidden layer was varied during development, whereas the last hidden, which was used as latent representations for subsequent networks, was kept fixed in size. All instances were feedforward neural networks, and all but the first so-called multilayer perceptrons (MLPs). Due to the local scope of each network during training and run-time (and the sparse splicing of input features), the networks, however, emulated the behavior of a CNN. The networks used the scaled conjugate gradient training method and were trained with batch gradient descent using the cross-entropy cost function.

N_x	Objective	Input from	Network output	Size	Val. stop
N_1	Detect tentative f_0 s	L	Tentogram	65-1	20
N_2	Classify tentative f_0 s	LN_1	Pitchogram	176-100-14-1	40
N_3	Detect onsets across pitch ridge	LN_2	Onset activation	1485-50-30-1	50
N_4	Detect offsets across pitch ridge	LN_2	Offset activation	1485-50-30-1	50
N_5	Determine most likely offset position	LN_2N_4	Offset curve	253-100-1	80
N_6	Classify notes	LN_2N_3	Note classification	2893-150-1	120

Table 3. Networks used by the system, their abbreviation, objective, input, output, size, and the number of epochs used for validation stopping.

All networks were trained with early stopping (*Val. stop* in Table 3), halting training after no more improvement could be achieved on the validation set. The number of failed epochs allowed before validation stopping was higher for later networks, to discourage too pronounced overfitting on the training set at an early stage. Furthermore, the spectrum of each ME-spectrogram was randomly varied in between the training of the networks (as described in Section 11.1) to promote generalization.

An overview of the run-time operation is provided in Figure 3. Although the networks were implemented as MLPs, the first layer emulates a sparse convolutional kernel at run-

time, with the output depth (the number of kernels) corresponding to the number of hidden neurons in the following hidden layer. This is due to the way in which the input was sliced across pitch and time with respect to the scalar target (local scope) of each training example. Continuing the analogy, subsequent layers of each network use 1×1 convolutional kernels extending across depth, with the number of kernels corresponding to the depth of the subsequent layer. The first two networks (N_1 and N_2) convolve across pitch, whereas the subsequent three networks (N_3 , N_4 , and N_5) instead convolve across time. As illustrated, the pitch ridge can fluctuate in pitch depending on detected tone information, facilitating tone-shift-invariance. Information associated with ridges is processed in several layers, using convolving across time. Although the offset detection network (N_5) and note classification network (N_6) also use inputs that are sliced across pitch and time, they receive input from so many representations that they instead were illustrated as MLPs.

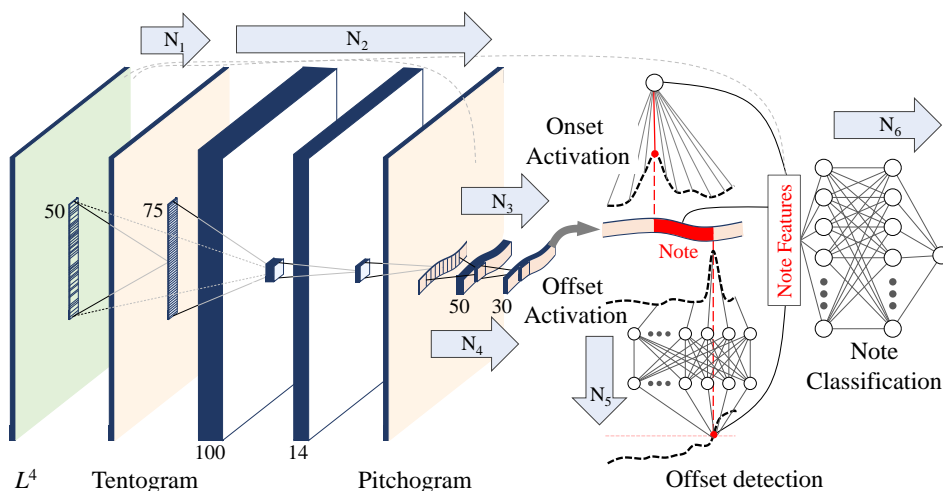


Figure 3. An overview of the networks used by the system at run-time, illustrating the processing steps as a combination of CNNs and MLPs. A sparse kernel convolves the spectrogram representation L^4 , producing a Tentogram consisting of tentative f_0 s. A deeper and bigger network (N_2) is applied to tentative f_0 s, using a similar kernel strategy for its first layer. An identified pitch ridge in the resulting Pitchogram is convolved across time by networks N_3 and N_4 to compute onset and offset activation curves. A detected onset and offset for a note is illustrated with red dots in the activation curves. It is shown how these points bound the extension of a note (red) across time. Spectral features are finally gathered across the extension of the note together with context information, and these collected note features are used for the note classification.

5. Computing the filtered spectrogram

5.1 Overview

The first step of the system was to compute a spectrogram representation for the f_0 -estimation that compensates for the time-varying sound level (at a phrase resolution) and the long-term cumulative average spectrum of the recording. These aspects of the audio vary depending on, for example, instrumentation and the dynamics of the performance (Elowsson and Friberg, 2017a). By compensating for the time-varying sound level, the same processing weights may be applied when estimating f_0 s at soft and loud section, thereby providing invariance to the level. By compensating for the long-term spectrum, the same processing weights may be applied when, for example, processing tracks played by instruments that vary in spectral characteristics such as the violin or piano, thereby providing some invariance to instrumentation. Such *spectral whitening* procedures are rather common in pitch tracking (see, e.g., Klapuri, 2006).

An overview of the filtering process (Section 5.3) and the resulting spectrogram is provided in Figure 4. The 2-dimensional matrix SV was computed to represent the long-term average spectrum up until each new time frame (pane 2), and the 1-dimensional vector LV was computed to represent the time-varying sound level (pane 3). These variables were combined to form the matrix LS (pane 4), the time-varying average spectrum. By subtracting LS from the initial spectrogram (Section 5.2, pane 1), the invariant spectrogram L could finally be computed (pane 5).

To make sure that the f_0 -estimation could be run in real-time, for example, during a live performance, the filtering was designed so that it could be applied in a time-casual manner with a relatively small delay (look-ahead) of 0.093 s (16 frames). However, since the subsequent note-tracking steps are not time-casual, the f_0 -estimation was not run as such either during evaluation.

5.2 Computing the initial spectrogram

The initial spectrogram was computed for each ME with the VQT (Schörkhuber et al., 2014), using 60 bins per octave and a frequency range of about 37 Hz-14.5 kHz. The parameter that controls the time-frequency resolution trade-off in the lower frequencies was set to $\gamma = 11.6$. The resulting magnitude spectrogram M had 518 log-frequency spaced frequency bins, and the hop size was 256 samples/frame, corresponding to 5.8 milliseconds (ms).

5.3 Filtering the spectrogram

Spectral variation (SV)

The spectral variation was computed both across frequency and time in a time-casual manner. Let M_k represents a spectrum vector of length 518 at a frame in time. The unfiltered spectral variation vector of the same shape, denoted by \widetilde{SV}_i was then computed at

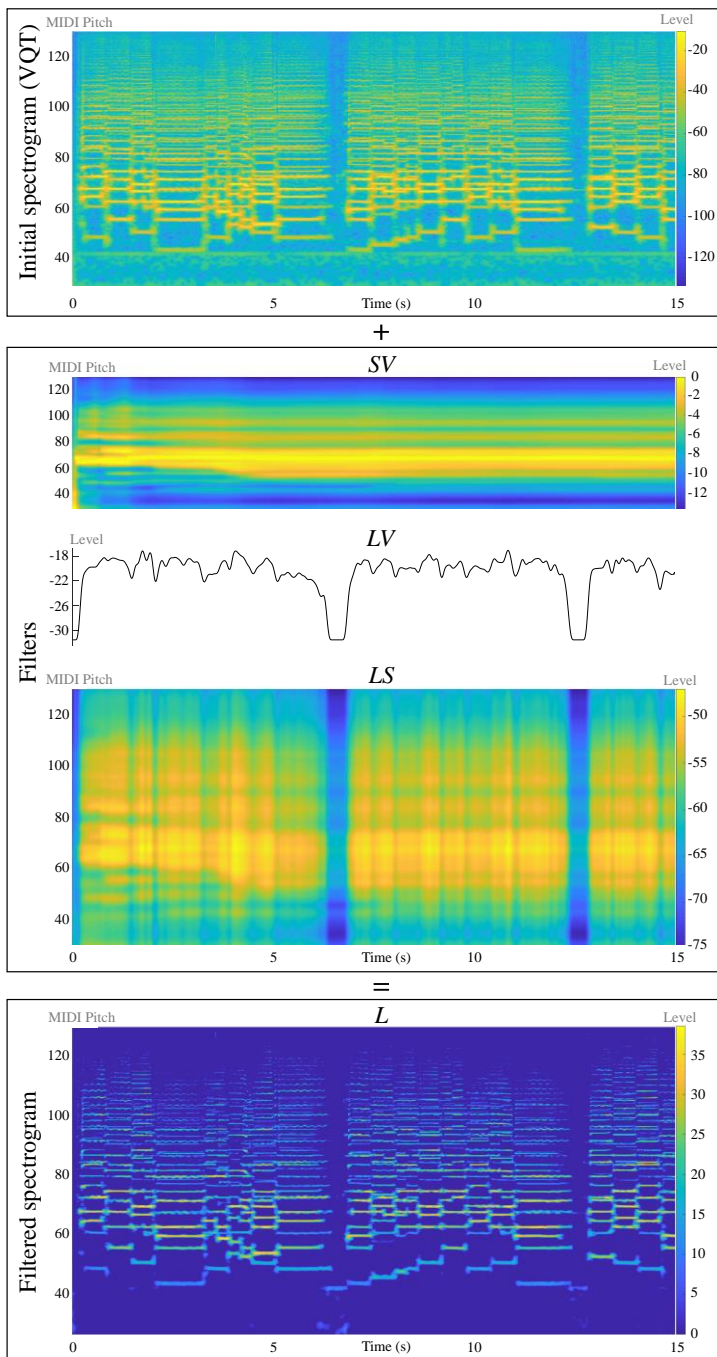


Figure 4. The initial VQT spectrogram, computation of LS from SV and LV , and the resulting output of the filtering, L . The spectrograms are shown for the first 15 seconds of ME No 1 of the Bach10 test set.

frame i by taking the mean magnitude of all previous frames

$$\widetilde{SV}_i = 20 \log_{10} \frac{\sum_{k=1}^i M_k}{i}. \quad (6)$$

For computational purposes, this was computed from the cumulative sum in each frame MC_k of the magnitude spectrogram

$$MC_1 = M_1, \quad MC_k = MC_{k-1} + M_k, \quad \widetilde{SV}_i = 20 \log_{10} \frac{MC_i}{i}. \quad (7)$$

After this, each frequency bin of SV_i was smoothed across frequency, using a Hann window with a width of 33 frames, centered at frame i . Finally, each frame was normalized with respect to the level, and the spectral variation reduced

$$SV_i = \frac{\widetilde{SV}_i - \max(\widetilde{SV}_i)}{3}. \quad (8)$$

Level variation (LV)

The sound level variation of the music across time was computed from the maximum bin-magnitude of each time frame (FM_i), and the cumulative maximum at each frame (CM_i):

$$FM_i = \max_{1 \leq j \leq 518} (20 \times \log_{10} M_{ij}), \quad CM_1 = FM_1, \quad CM_i = \max\{CM_{i-1}, FM_i\} \quad (9)$$

However, for the main evaluated model (non-time casual), CM_i was replaced with the maximum across the whole track. This was the only difference between the time casual and non-time casual f_0 -estimation. From a listener's perspective, the cumulative maximum gives a (time-casual) indication of a reasonable playback volume for the track, whereas the framewise maximum (crudely) indicates the local loudness of the track. Note that SV was computed in a time casual manner for both versions. The two variables FM_i and CM_i were combined into LVF_i , a compromise between local and global (up to time frame i) considerations, where H represents smoothing across time with a Hann window of size 33

$$LVF_i = H(\max\{FM_i, CM_i - 30\}). \quad (10)$$

The output of Eq. 10 was then combined with a time-shifted copy of the cumulative maximum

$$LV_i = \frac{LVF_i + CM_{i+16}}{2} - 6, \quad (11)$$

to form LV . A reason for applying Eq. 11 is to avoid an increase of LV in tandem with the increased loudness from the first tones (or from the first loud section) of a track. By increasing LV before the increase in loudness of the track, onsets will not be disguised by the change in the noise floor. Of course, the best solution would be to establish the noise floor of the complete track before continued processing, but this is not possible in a time-casual implementation.

Combining LV and SV

The noise floor LS was computed for each time frame by multiplying the scalar LV_i with the vector SV_i . Then, the filtered spectrogram was computed, using three different ranges:

- $L = \max\{(20 \times \log_{10} M) - LS, 0\}$,
- $L_{15+} = \max\{(20 \times \log_{10} M) - LS + 15, 0\}$,
- $L_{25+} = \max\{(20 \times \log_{10} M) - LS + 25, 0\}$.

In the system, L was used for f_0 -estimation, L_{15+} for onset detection, and L_{25+} for note classification. The reason for initially using L , which may discard relevant information, is that, for computational purposes, a linear combination of spectrogram levels is used for the Tentogram. Therefore, the values should reflect the relative importance of the respective magnitudes in the spectrogram. For onset detection, this restriction no longer exists, and information at lower signal levels can be provided.

After filtering, the frequency dimension of L was upsampled to four times its original size with linear interpolation, creating the spectrogram L^4 .

6. Tentogram

6.1 Overview

A refined model of pitch, and pitch interaction across frequency, is necessary to accurately transcribe polyphonic music. To account for time-varying tonal information, f_0 s needs to be computed with a sufficient resolution both across time and frequency. There is a significant computational cost associated with this if the processing is to have the necessary complexity. Therefore, the pitch detection step was divided into two sub-steps in the system. First, rough tentative pitches were computed using a computationally fast spectral summation (to produce a Tentogram), and then detected f_0 -candidates were further evaluated (to produce a Pitchogram as described in Section 7).

The Tentogram network (N_1) was trained to estimate framewise f_0 s from spectral energies in bins sparsely distributed across frequency in L^4 . The frequency offset of these bins was initially learned by the network (Section 6.3), and the network can be described as a single sparse convolutional kernel. However, additionally, a set of 15 DCT components, extracted at each f_0 training example (Section 6.2), were used to infer a Tentogram whitening (Section 6.5). Weights were inferred by a neural network using no hidden layers⁷, and these were used to specify a computationally efficient run-time operation (Section 6.6) that produces the final Tentogram. The weight sharing mechanism of the kernel has similarities to that of receptive fields in CNNs. For image processing, weights are shared across adjacent pixels. Auditory perception of music however differs in that, for example, octave-spaced frequency bins are more closely related. An overview of the network used to compute weights for spectrogram summation and Tentogram whitening is shown in Figure 5, with input, weights, and output, for making a prediction of a single

⁷ This is very similar to logistic regression, but a neural network implementation with a sigmoid activation function was used for computational purposes.

pitch bin. The produced Tentogram had 1563 frequency bins and a pitch resolution of 5 cents/bin.

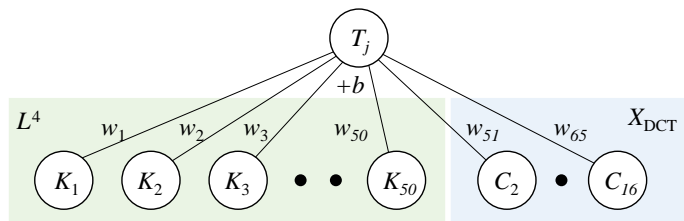


Figure 5. Inferring weights for spectrogram summation and Tentogram whitening. Weights were computed for 50 bin offsets, and 15 DCT components.

6.2 Extracting f_0 training examples

A set of correct and incorrect f_0 s were extracted for each voiced frame of the MEs in the training set. These were used to generate training examples for the network, as it would be excessive to train with all 1563 frequency bins – many of which are easy to dismiss and therefore rather irrelevant for training. Training was repeated two times, with a slightly different way of selecting training examples for the first and second iteration. In the first iteration, the annotated f_0 s (T_A) were used for the true class in the network classification, and the false class T_F consisted of training examples at $\pm\{3\ 4\ 5\ 6\ 7\ 8\ 9\ 12\ 19\ 24\}$ semitones relative to each annotated true f_0 (in each time-frame). Any T_F within 50 cents of a T_A in the time-frame was removed.

After training the kernel in the first iteration, the system was executed with the trained kernel, and a Tentogram computed for each ME. The computed tentative pitches were then used to provide additional and improved training examples. In this case, for each annotated f_0 , the closest pitch detected in the tentogram was used to replace the actual annotation, if a relevant pitch (within 50 cents) could be found. This is useful, as vibratos or other smaller pitch shifts are not included in the annotations generated from the MIDI files. The same technique was used to improve the pitch of the false training examples at the previously specified pitches. Furthermore, any additional false pitches detected in the Tentogram were added to T_F as false annotations, so that these could be suppressed as well.

6.3 Learning the pitch kernel

The tentative pitch activation for all pitches was computed with a weighted sum of relevant frequencies of L^4 in each time-step. Which frequencies could be the most useful in this regard? Relevant frequencies are arguably those that correspond to pitch partials of an evaluated f_0 , as well as other frequencies that could be used for indicating that a certain pitch is incorrect, e.g., an octave error. The other frequencies will be referred to as inter-partial, positioned in between the partials, and at subharmonics of an evaluated f_0 . A simple assumption is that f_0 s that have *overlapping* partials are more likely to be mixed

up with each other, resulting in an erroneous transcription. Therefore, the frequency of the *non-overlapping* partials of easily confused f_0 s should also be included as features.

The most obvious inter-partial frequencies are those with simple ratios in relation to the evaluated f_0 . For example, pitches at an octave below, a fourth below and a fifth above an evaluated f_0 all have partials that overlap the first harmonic of that f_0 . However, with increasing polyphonic level (and harmonic complexity), the number of inter-partial necessary to untangle the mesh of overlapping partials in the spectrogram increases. Relevant inter-partial will also vary with musical styles, instrumentation, and the noise profile of the audio recordings. It is very likely that a manual selection would lead to mistakes, omitting some useful inter-partial indexes, while including those that may not contribute to a higher predictive performance. This would lead to a higher computational cost and a lower performance. Therefore, the inter-partial positions were instead learned directly by the system. Given the run-time behavior of the tentogram network, the system can be conceived as using a learned sparse *partial receptive field* or *pitch kernel*. This pitch kernel is used for many important computations throughout the system.

The kernel K , consisting of bin-offsets K_B with the corresponding spectrogram levels K_L extracted from L^4 , was initialized with the first 11 partials of the f_0 ($K_{\text{size}} = 11$). This was done under the assumption that, even if these frequencies cannot contribute during the linear combination for the Tentogram, they should all be relevant during the subsequent non-linear processing for computing the Pitchogram. The bin-offset of the n th partial was computed from

$$\lfloor \log_2(n) \times bpo \times uf \rfloor, \quad (12)$$

where bpo represents the number of bins per octave of the VQT (60), and uf represents the upsampling factor (4). The operation $\lfloor x \rfloor$ is used for rounding the result to the closest integer. An important benefit of using the upsampled spectrogram L_4 is the reduction of these rounding errors, which ensures that partials and learned inter-partial are added with a high precision.

Inter-partial were then chosen by forward selection, iteratively adding each inter-partial to K_B , evaluating the performance with K_L as input to the network, and finally choosing the inter-partial that improved performance the most after all had been evaluated. Inter-partial were selected from -40 to $+45$ semitones (around 7 octaves) relative to the f_0 . The resolution was 20 bins/semitone, so the number of inter-partial was $85 \times 20 = 1701$, and the number of inter-partial evaluated in each iteration of the forward selection procedure was $1701 - K_{\text{size}}$.

To reduce the computational cost, each iteration was performed in two separate steps - a fast step using fewer training examples, and a second step for the most relevant inter-partial with more training examples. In the first step, every 2900th time-frame in the training set was used for training, and every 500th frame of the validation set was used for validation. The Tentogram network was trained with early stopping and the performance for each variation of K calculated. The result was added to a performance vector X , of length 1701. Values at bin offsets already added to K_B were determined by interpolation of neighboring values. The vector X was then smoothed with a Hann window of size 13,

and the 45 lowest values (best performance) further evaluated in the second step. The smoothing reduces the variability, which can be expected to be high due to the small size of the training set in the first step. If neighboring bins perform well, a test for the larger training set could still be meaningful. For the second step, every 100th frame of the training and validation set was used, and the best performing of the 45 evaluated bin offsets added permanently to K_B . The forward selection was set to halt when four iterations had not produced an improved performance, or when $K_{size} = 50$. During the first training run used for created improved training examples (Section 6.2), the maximum number of bin-offsets was instead set to 30.

After the pitch kernel had been defined, the network was finally trained with more data, using every other time frame from the training and validation set. The bias term (constant) determined from the network during training will be denoted K_C , and the computed weights K_W .

6.4 Bin offset distribution of the learned kernel

The 50 bin offsets of the pitch kernel (11 pre-determined, 39 determined during training) are shown in Figure 6. They range from -705 to 874, with 17 of the learned offsets being negative and 22 positive. The distribution indicates that, excluding pre-determined partial positions, bins below the f_0 in the spectrogram are roughly as important as bins above the f_0 for the system.

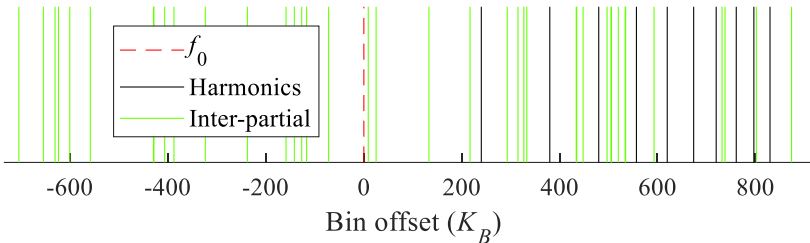


Figure 6. The bin offsets (K_B) used by the pitch kernel, at a resolution of 5 cents/bin. The partial positions (black vertical lines) were pre-specified and the inter-partial positions (green vertical lines) were learned during training.

There seems to be an interesting pattern for the learned part of the kernel; the network repeatedly selected bin-offsets at a frequency ratio relative to the f_0 corresponding to fractions of small prime numbers. Such prime pair fractions for small primes {2 3 5 7 11 13} are presented in Table 4. The reason for selecting fractions corresponding to low integer factors for the frequency ratio is easy to understand. Notes in Western tone scales produce many partials at such ratios. However, it remains to be studied whether factor-pairs with one non-prime small integer factor {4 6 8 10 12} are as common as prime-pairs, relative to the number of simplest-form fractions that they occur in.

Fraction	Ideal bin	Found bin
7/11	-156.5	-159
2/3	-140.4	-142
5/7	-116.5	-117
13/7	214.3	217
7/3	293.4	293
5/2	317.3	315
13/5	330.8	333
7/2	433.8	434/435
11/3	448.9	448
13/3	507.7	505/506
11/2	590.3	593

Table 4. Fractions of prime integer factors relative the frequency of the f_0 , learned for bin offsets. Eleven small prime pairs were discovered within 15 cents of the ideal bin offset for a prime pair.

As can be seen in the table, sometimes neighboring bins were used by the system. This happened four times for the kernel, and each time, one of the bins was assigned a relatively large positive weight and one a relatively large negative weight. These bin-pairs, therefore, act as an edge detector on the spectrogram. The effect is that they can suppress or increase the likelihood of an f_0 based on the slope of the spectrogram level (across frequency) at the given offset. Further analysis of the learned bin offsets, while interesting and important, is beyond the scope of this article.

6.5 Tentogram whitening learned from DCT components

As input to the network, K_L was complemented with the value of 15 DCT components representing the pitch of the t_0 . This enabled the network to whiten the Tentogram representation using a compressed representation. The solution solves two problems:

- It can be assumed that the linear combination of spectrogram bins at various offsets will produce more false activations at some pitch ranges than others. For example, harmonics at the higher pitch range may not always be sufficiently suppressed; and the more densely populated range around the middle C (MIDI pitch 60) may not be sufficiently elevated.
- The pitch of the t_0 cannot be used as an input feature to express anything but a low pitch/high pitch preference, due to the linear processing of the network. The first components of the DCT can, however, express preference across the pitch range, at a smoothness varying with the number of components included.

First, a precomputed basis function B_{DCT} of size 15×1563 was formed by the first 15 components of the DCT III (excluding the constant DC component), as shown in Figure 7. The values of the coefficients were adapted to be similar to the range of values in K_L , using a scale factor of 35. For each training example, the index position i into B_{DCT} was derived from the MIDI pitch P according to

$$i = (P - 25.8) \times 20 \quad 1 \leq i \leq 1563, \quad (13)$$

and a vector, X_{DCT} , of 15 components was extracted.

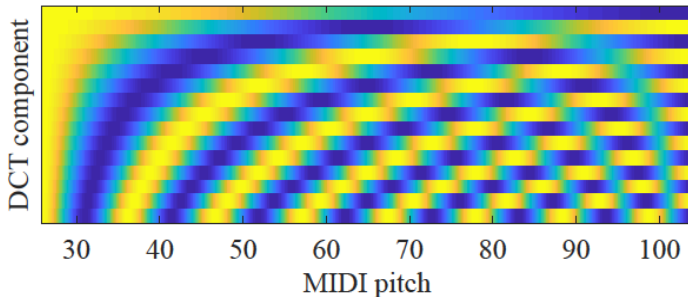


Figure 7. The B_{DCT} from which the input vector X_{DCT} is extracted. This input vector consists of 15 DCT components and is used by the network to whiten the Tentogram across pitch.

The vector X_{DCT} was included as input to the network, both during the kernel forward selection and the final training. The whitening vector was finally derived from the matrix multiplication

$$W = W_{DCT} \times B_{DCT}, \quad (14)$$

where W_{DCT} corresponds to the computed weights for X_{DCT} from the network. The whitening vector, shown in Figure 8, was added to each frame of the Tentogram as specified in Section 6.6 (Run-time).

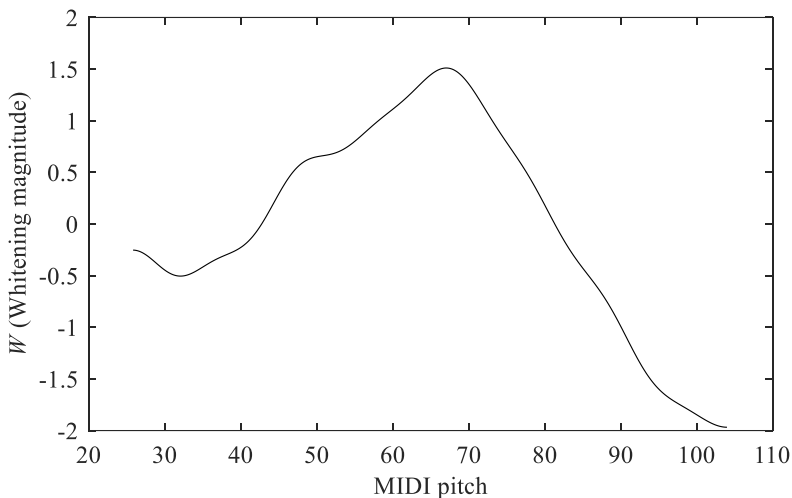


Figure 8. The Tentogram whitening vector W computed during training. The system learned to give lower weight to high pitches, and higher weight to two octaves around MIDI pitch 65.

6.6 Run-time

At run-time, the summation of partials and inter-partial of the kernel was done by summing K_{Size} copies of the 2-dimensional spectrogram L^4 . First, each copy was shifted $-1 \times K_B$ frequency bins, bins outside of the corresponding MIDI pitch 25.85-103.95 discarded, and potentially missing rows of bins in a copy padded with zeros. This resulted in the 3-dimensional matrix L_K^4 . Each copy was then weighted according to its computed weight K_w by multiplication, and the copies summed. This operation was done with a simple matrix multiplication, $K_w \times L_K^4$, where K_w had the size $1 \times K_{Size}$ and L_K^4 the size $K_{Size} \times 1563 \times nf$. The number of time-frames in the ME is represented by nf . Using matrix multiplication to compute the tentogram ensures computational efficiency. Note also that the processing generates a Tentogram activation for every pitch bin. The run-time behavior thus differs from the training procedure, which only extracts the most relevant pitch bins for training (the true f_0 s and the false f_0 s most likely to be erroneously activated).

The constant bias weight from the network training K_C and the whitening vector W were summed into a vector

$$V = W + K_C + 3.5, \quad (15)$$

which was added to each time frame after matrix multiplication. All values below 0 were then set to 0. The addition of 3.5 ensures that rather improbable tentative f_0 s also are processed by the subsequent pitch network. The Tentogram T was finally derived by filtering with h , a 2-dimensional Gaussian $\sigma = 3$, truncated to the size of 11×11 bins ($64 \text{ ms} \times 0.55$ semitones).

In early experiments of this study, the performance was also evaluated when only summing those instances of the pitch kernel where partials were detected. In this case, peaks were detected from linear- or log-frequency spectrograms, and frequency shifted according to the kernel. The methodology seemed to result in slightly better performance for instruments with clearly marked partial peaks (i.e., instruments without vibrato). However, performance was lower for instruments with stronger pitch shifts. Friberg et al. (2018) used an early version of the partial summation method for predicting articulatory categories.

7. Pitchogram

Peaks were detected in the Tentogram (T) in each frame i as the pitch bins j where $T_{i,j} > T_{i,j-1}$ and $T_{i,j} > T_{i,j+1}$. Detected peaks defined tentative f_0 s (t_0 s), and these t_0 s were evaluated in a second, larger network (N_2). By using parabolic interpolation, the pitch of each t_0 was estimated to a resolution of 1 cent. The input layer (described in Section 7.1) to the network for each t_0 consisted of the respective kernel levels (K_L), the max pooled kernel levels, and the activation level of t_0 s in the frame, at semitone intervals. Each t_0 was evaluated as *true* or *false*, and the N_2 network trained to classify them. Just as for the Tentogram, the weight sharing of the first layer of a CNN was emulated by extracting the

input layer for each training example at indices relative to the t_0 , while training with a fully connected neural network. An overview is given in Figure 9, and details provided in Sections 7.1-4.

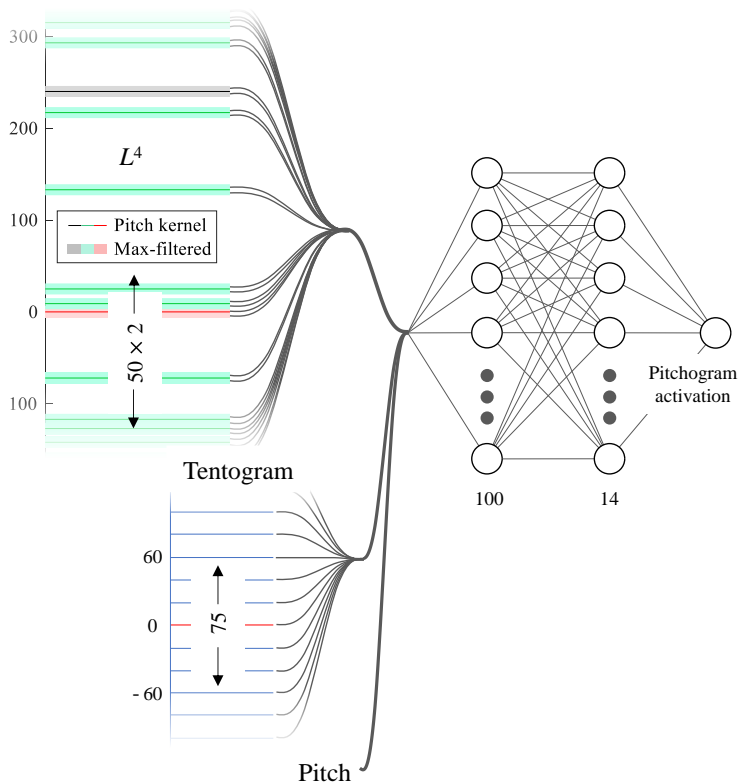


Figure 9. The input to the pitchogram network used to compute the pitchogram activation for a processed t_0 of a single frame. Red lines indicate the t_0 . For the L^4 spectrogram, black is a pre-defined offset at the first harmonic, and green is learned inter-partials in K_B . For the Tentogram, blue is the semitone offsets at which the maximum of close t_0 s is extracted. All features are connected to all neurons in the first network layer. As the same process is applied to all activated tentogram bins, the processing is functionally reminiscent of a convolutional layer applied sparsely across the Tentogram.

7.1 Network

Input

The K_L , previously used for training the Tentogram network (Section 6.3), was extracted by taking a cross-section of L_K^4 at frame i , and bin j . Essentially, this representation is used as a skip connection, motivated by the fact that the learned bin offsets K_B at which K_L are extracted are rather optimal for the task. Additionally, a “pooled” (maximum magnitude across frequency) version of the same features was used. The idea behind the pooling procedure was to account for variation, while also implicitly giving a hint to the

network of the approximate absolute distance between existing partial peaks in the spectrogram and partial and inter-partial frequencies defined in the pitch kernel⁸. The maximum level was extracted at ± 6 bins in L_F^4 , corresponding to ± 30 cents.

The maximum t_0 -peak was extracted at ± 36 semitones relative to each evaluated t_0 . One value was computed for each semitone taking the maximum t_0 at ± 50 cents. For semitones where no t_0 could be detected, the value 0 was used. The sum of all $t_0s > 36$ semitones and all $t_0s < -36$ semitones was used as two additional input features. Finally, the pitch of the processed t_0 was also added as an input feature.

Training Procedure

Each t_0 was evaluated as *true* or *false* by the evaluation procedure presented in Section 2.3. Any t_0s within 50 cents of an annotation that had been classified as false during evaluation were discarded from training. Two hidden layers were used (size 100 and 14) to provide modularity regarding the size of the network while keeping the last hidden layer fixed in size.

7.2 Maximized framewise F-measure - \mathcal{F}_{fr}

After training the network, the threshold that maximizes the framewise F-measure (\mathcal{F}_{fr}) was computed for the *validation set*. First, the network was applied to each extracted t_0 of the validation set, computing the activation Z . The threshold was incremented in steps of 0.01 over the relevant range, and at each step \mathcal{P} , \mathcal{R} and \mathcal{F}_{fr} (see Section 2.3) were computed for the validation set. The vector of \mathcal{F}_{fr} -values computed at incremented thresholds was smoothed with a Hann window of size 71, and the threshold at the maximum \mathcal{F}_{fr} determined. Applying this threshold results in the \mathcal{F}_{fr} measure, used (only) in the evaluation of the training set⁹.

7.3 Run-time

Due to the input structure, the network at run-time can be understood as an initial layer with 100 convolutional filters, followed by 14 1x1 convolutional filters having a depth of 100 (see N_2 in Figure 10 of the overview). First, t_0s and the corresponding input features were extracted, and an activation computed for each t_0 from the trained network. The value prior to the sigmoid activation function of the output layer was used, and the constant 3.6 added. This value was selected under the assumption that activations for rather unlikely t_0s could also provide valuable information. All activations below zero were discarded, and the remaining activations inserted in the Pitchogram at the pitch-bin corresponding to the previously interpolated pitch of each t_0 . The Pitchogram was smoothed across pitch with a Hann window of size 41. The threshold optimized on the validation set for \mathcal{F}_{fr} was also applied, and the result saved for evaluation. Figure 10 shows the spectrogram L , the Tentogram computed from L , and the Pitchogram (optimized for \mathcal{F}_{fr})

⁸ If there is a partial peak close to the kernel frequency, the difference between the pooled and non-pooled signal level gives an indication of the absolute frequency distance between the kernel frequency and that partial peak.

⁹ The main evaluation for the test sets were instead based on the framewise note estimates, as described in Section 10.4.

computed from earlier representations, for 6 seconds of audio. As shown, the 2-step process gradually refines the estimates while upsampling the resolution, unveiling, for instance, vibratos. There are very few activations outside annotated notes, and all annotated notes have a corresponding activation. The most challenging tone is the bassoon pitch 57 in the center of the excerpt, as the fundamental partial has very little energy while the second partial is very strong.

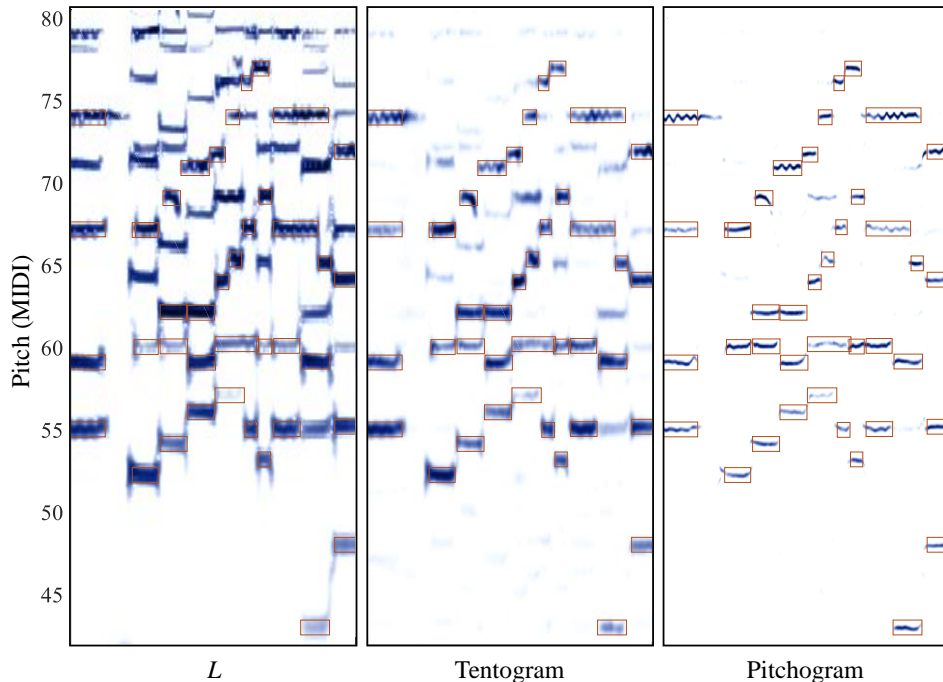


Figure 10. The filtered spectrogram representations L , computed Tentogram, and the Pitchogram optimized for \mathcal{F}_{f_0} for 6 seconds of audio (time points 18 to 24) in Bach10 ME No 1. Ground truth annotations based on onset and offset times are marked with a red rectangle (these are sometimes slightly incorrect). The clean and high-resolution Pitchogram is achieved through up-sampling during the layered learning process.

7.4 Detecting regions in the Pitchogram

Regions of f_0 -activations were extracted from the Pitchogram, to facilitate further processing. This was done by converting the thresholded Pitchogram into a two-dimensional binary image, and then identifying connected components in that image. A connectivity of eight was used, meaning that each above-zero pixel in the image could be connected to all eight surrounding pixels.

Subsequently, regions with a similar pitch that follow in close succession were merged. This was done to be able to track f_0 -activations over a longer period of time, even if some parts briefly go below the threshold. The pitch of each region was first computed as the weighted centroid of its f_0 -activations. Then, for each region, ordered based on start time,

any new region with a pitch within 50 cents of the old region and with a start time between 0 and 130 ms after the old region was merged to form a combined larger region. The merging was done in an iterative procedure, updating the pitch, onsets, and offsets of regions after each merging.

Some of the extracted regions will cover several seconds, while some just consist of a few pixels. All regions with a summed f_0 -activation below 100 were removed before merging, and all regions with a summed f_0 -activation below 300 were removed after merging. These regions are so small that they are very unlikely to represent a true underlying note pitch. A summed f_0 -activation of 100 corresponds to a single isolated f_0 -activation of 0.68 before processing the pitch network output (removing output activation and smoothing).

In image processing, similar types of regions have often been referred to as “blobs”. Most similar to our proposed technique is the system for audio-to-score alignment proposed by Miron et al. (2014), which relied on blob-detection from pitch-salience estimates, using start-points and end-points of the blobs as onsets and offsets.

In the next step, a ridge was extracted for each region and the onset detection was applied along this ridge. For each time frame, the pitch index of the ridge corresponded to the maximum f_0 -activation, using the same resolution of 1 cent as in the pitchogram. If no pitch activation was present for a specific time frame, the pitch index was determined by linear interpolation between detected pitch indexes before and after the evaluated time frame. The ridge was also extended backward 30 frames before the first time-frame of the region. These frames were assigned the same pitch index as the first frame of the region (nearest neighbor extrapolation). Figure 11 shows the pitch ridge (red line) extracted from a merged region and a non-merged region. The pitch ridge extends horizontally at the edges of the two regions (extrapolation) and connects regions at edges during interpolation. The abrupt incline upwards at 5.7 seconds is a result of a spurious small (erroneous) region being merged in between bigger regions.

Finally, the pitch activation was computed for all frames of the ridge where the pitch activation had not previously been computed for that pitch index. After this, each region had been assigned a one-dimensional ridge across time, which was used to compute an onset and offset activation curve. As the ridge traces the pitch fluctuations, the subsequent processing will benefit from an accurate and high pitch resolution, while being invariant to local pitch variations of the tone. This tone-shift-invariant (or vibrato-invariant) property of the system promotes generalization across instrumentation – differences in tone stability are negated when tone features at each time frame are extracted relative to the established pitch ridge (see Section 3 – *Disentangled structures*).

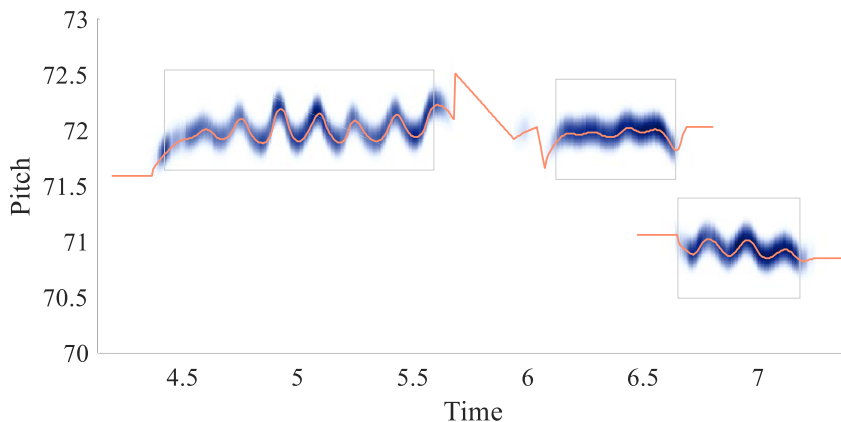


Figure 11. Merged pitch regions (MIDI pitch 72) and a single region (MIDI pitch 71), with the corresponding pitch ridge (red line) from which onsets and offsets were computed. The notes were played by the violin and are from the four-voiced ME No 2 of the Bach10 test set. Ground truth annotations are marked with a grey box.

8. Onset detection

An onset activation function was computed with a neural network (the onset network N_3) along the ridge of each detected region. The input to the network was mainly the change in activation or signal level across time for previously computed representations. This included the *neural flux* (NF), the absolute *pitch flux* (PF) and the *spectral flux* (SF), all described in the following subsections. Computing changes in activations or signal level provides an additional layer of invariance. If the values at which these changes happen are less relevant than the magnitude of the changes, this pre-processing can increase performance, as it relieves the network from inferring this connection across the whole input vector. However, the real values were also provided at a single time-frame, to provide the network with more complete information. Various combinations were tested during development, and this setup gave the highest results. The input structure is described for each time-frame of a ridge, and it was identical for all frames of the ridge. The processing of the first layer can therefore be understood as a convolutional layer, where the pitch-varying ridge defines the dimension that the convolution was performed over. In the overview of DLL (Section 2), this is defined as a disentangled structure for invariant processing.

8.1 Neural flux

The preceding pitch network is trained to activate at corresponding pixels between the start and end of each tone. Pitch activations along ridges will therefore generally rise at the start of new notes. It is intuitive to include these pitch activations so that the network can infer the presence of a note onset from them. For each time-frame, the activations at ± 40 frames were included, using a step size of two (discarding every other frame). This

time indexing will be referred to as T_2 in the rest of the article. The time-indexing for onset features generally skipped frames. As the time resolution was very high, this is just a way to reduce the size of the input layer while providing a sufficient context around the onset. It is the same strategy for time used by the earlier networks for pitch skipping some frequency bins.

Ideally, the activations from the output layer of the f_0 -network would be enough to identify onsets. However, accurately detecting all present fundamental frequencies can be very hard, not only for computer models but also for skilled listeners; especially in dense polyphonic textures. It can therefore be expected that activation patterns in the Pitchogram will be insufficient to detect onsets accurately. As listeners get the benefit of tracking music along time, they may however still be able to hear pitch onsets by relying on various clues, for example regarding how harmonics vary in loudness across time. Clues of these types can also be expected to be encoded deeper in the layer-wise structure of the previous pitch network. Perhaps one neuron activates when detecting odd harmonics, while another neuron responds when there is a potential octave-error at the given pitch. Tracking these neural activations across time should be useful, providing more detailed information during the onset detection. Therefore, the NF from the 14 neurons of the last hidden layer of the pitch network was also used as input for the onset detection-network. Here a slightly smaller context window T_1 was used, corresponding to time frames (in relation to the evaluated frame) of $\{-13 -8 -4 -2 0 2 4 8 13\}$.

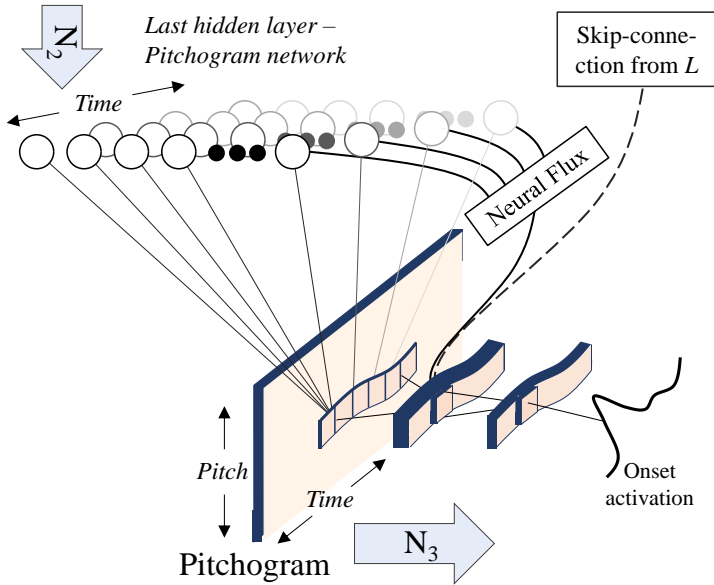


Figure 12. The last hidden layer of N_2 for different time-frames that have been connected as they belong to the same pitch ridge. The fluctuation in activation from each neuron is computed across time and used as input for computing an onset activation in N_3 . The output activations of N_2 , and the SF from L are also included as input.

The fluctuations were computed as the difference between each frame in T_1 for each individual neuron. Furthermore, the original activations of the evaluated time-frame (frame 0) were also included, providing context about the raw values at which activations changed. Figure 12 illustrates how the output from different time-frames of the same neuron in the last hidden layer of N_2 are sent to the neural flux function. This function computes a vector containing differences in the output and sends this to the input of N_3 . Other representations used for computing the onset activation are also included in the figure.

8.2 Spectral flux

Although the NF should capture many of the relevant changes in the spectral characteristics that can be associated with note onsets, the objective of the pitch network was never to track these onsets. In many instruments, the spectral characteristics vary considerably during an onset, and the spectrum is not the same as in the subsequent steady part of a note. Therefore, a more low-level representation was also supplied to the network, in the form of the SF, computed from L_{+15} . The SF was computed using frequency bins relative to the ridge frequency between -186 (down three octaves and a semitone) and +306 (up five octaves and a semitone), using every other bin. This index will be referred to as F_1 . To also account for information at skipped bins, the spectrum was first smoothed across frequency with a vector of length three {0.25 0.5 0.25}. Relative time indexes {-12 -8 -4 0 4 8} were used (T_4), computing the difference over every other index (i.e., the SF between frames -12 and -4, between -8 and 0, etc.). Furthermore, the signal level at the evaluated frame (frame 0) was also provided. As argued previously, this provides additional information about the loudness at which the relative changes occur.

8.3 Pitch flux

The absolute pitch flux (PF) was computed for the time-varying ridge-pitch P , at all time-frames i of the context window T_2 by

$$|P_{i+1} - P_i|. \quad (16)$$

As defined in Eq. 16, absolute difference was used, so features did not differ between a falling or rising pitch. The intuition is that information about the *presence of a fluctuating pitch* is much more valuable for the task than information about the direction of potential pitch fluctuations. By using the absolute value, the network can use the same processing for both cases, building invariance into the system. The pitch of the region was also provided as an additional feature.

8.4 Additional features

Information of the loudness variation (LV) computed in the preprocessing of the spectrogram was provided. The change (derivative) of the LV was provided across indexes T_2 . Note that it is important not to provide raw LV values to the system because that would reveal the overall level of the audio file. The network would then make assumptions based on information (e.g., microphone gain) that is not musically relevant. Such incorrect assumptions lead to reduced performance for test tracks at another overall level than the

training set. As two additional features, the local time index in the region was provided, and the distance to the end of the region.

8.5 Training

The onset network was trained to classify whether a certain time-frame of a ridge corresponded to a note start or not. The ridge frames annotated as true (1) for training fulfilled the following criteria:

- identical time as the onset time of an annotation (when quantized to 256 samples/s),
- a pitch within 55 cents of that annotation.

The surrounding time-frames (± 7 frames) in the ridge were discarded from training. The rest of the frames were set to false (0). To obtain a more even balance between true and false annotations during training, about 95 % of the training examples annotated as false were excluded from training. The removed examples were chosen randomly. Settings during training are provided in Table 3.

8.6 Peak-picking onsets

The neural network was applied to each frame of a ridge, producing an onset activation curve (OC). The sigmoid output activation function used during training of the network was excluded during run-time. The OC was then filtered with parameters determined from a grid search on the training and validation set. The first step of the filtering was a thresholding operation, applied on each frame x of the OC by using a smooth thresholding function:

$$x = x - t - r \quad (17)$$

$$x = \begin{cases} r \left(\frac{e^x}{r} - 1 \right), & x < 0 \\ x, & x \geq 0 \end{cases} \quad (18)$$

$$x = x + r \quad (19)$$

The threshold t was -4.8, and r , stipulating the range within which the threshold smoothly takes effect, was set to 1. After this, the OC was smoothed with a Gaussian, using $\sigma = 2.8$. Finally, all peaks above 1.2 were extracted as onsets. To determine the parameter values, the recall (\mathcal{R}) and precision (\mathcal{P}) of the onset detection was computed for each combination of parameters. The function

$$S = 28.6 \mathcal{R} + \tan(2\mathcal{P} - 1) \quad (20)$$

was then applied for each combination, assigning much higher importance to \mathcal{R} than \mathcal{P} . This ensures a high recall in the onset detection; the precision was improved at a later stage when a sufficient context for each note had been collected. The tangent function acts as an inverted s -function in the applicable range, discouraging too low precisions (below around 0.25). The parameters that maximized S were then used, as previously

presented. The onset curve after filtering will be referred to as *OCS*. Exact onset times were determined with parabolic interpolation, using neighboring values in the smoothed *OCS*.

9. Offset detection

For each tentatively detected onset, an offset position was also computed. This was done in two stages. First, the same features and network size used for onset detection were also used for a network (N_4) producing an offset curve (*OFC*). Offset positions for each region were annotated by using a Hann window with a width of 13 frames and a maximum amplitude of 1, centered at the annotated offset position. This design was chosen due to the higher uncertainty in timing for offset positions.

A straightforward solution would have been to then choose offsets based on a peak-picking on the *OFC*. However, this approach could lead to missed offset for tones with slowly decreasing sound levels, or tones in dense polyphonic textures with a lot of uncertainty. If this were to happen, the offset position would have to be set to the end of the region, or just before the start of the next tone in the region. Therefore, to get a small average absolute distance between the annotated and computed offset position, a second stage, the offset detection network (N_5), was incorporated. For the annotations of this stage, the frames before the annotated offset for a detected note were set to 0, and frames after the annotated offset were set to 1. During five frames centered at the annotated offset position, a linear increase from 0 to 1 was used. Features accumulated from the start of the tone were then supplied to the network during training. The desired outcome is for the network to take accumulated evidence of an offset into account, with the output activation reaching 0.5 for the first time close to the annotated offset, subsequently increasing.

All falsely detected notes were discarded from the training set, to reflect the fact that no proper annotation could be assigned for these notes. The annotation associated with each detected onset was then also used to set the annotated offset position. If another annotated note offset of the same pitch (± 50 cents) occurred after the detected onset position but before the annotated offset position of a note, that note was also discarded from the training set. Finally, if a new annotated onset of the same pitch started within four frames of the annotated offset, the last four frames of that note were discarded from the training set. This was done to discourage the network from inferring offset positions by trying to find subsequent onsets.

Features for offset detection were computed by accumulating activations/magnitudes for the note along time, while also providing the present activation/magnitude. The futures for each time-frame were:

- The neural activations of the last layer of the pitch network, also using the cumulative mean of these activations.
- The output activation of the pitch network at relative time-frames given by T_1 , and a feature consisting of the cumulative mean (up to the time-frame) of these activations.

- The offset curve, *OFC*, at relative time frames given by T_1 , and a feature consisting of the cumulative sum of these activations. Furthermore, two more cumulative sums were computed by first subtracting 0.1 and 0.2 from the *OFC*, thresholding at 0.
- The pitch kernel signal levels used as input to the tentogram and pitch network, and a feature consisting of their cumulative mean.
- The pitch, the frame index (starting from 1 for each note), and the region index (starting from 1 for each region).

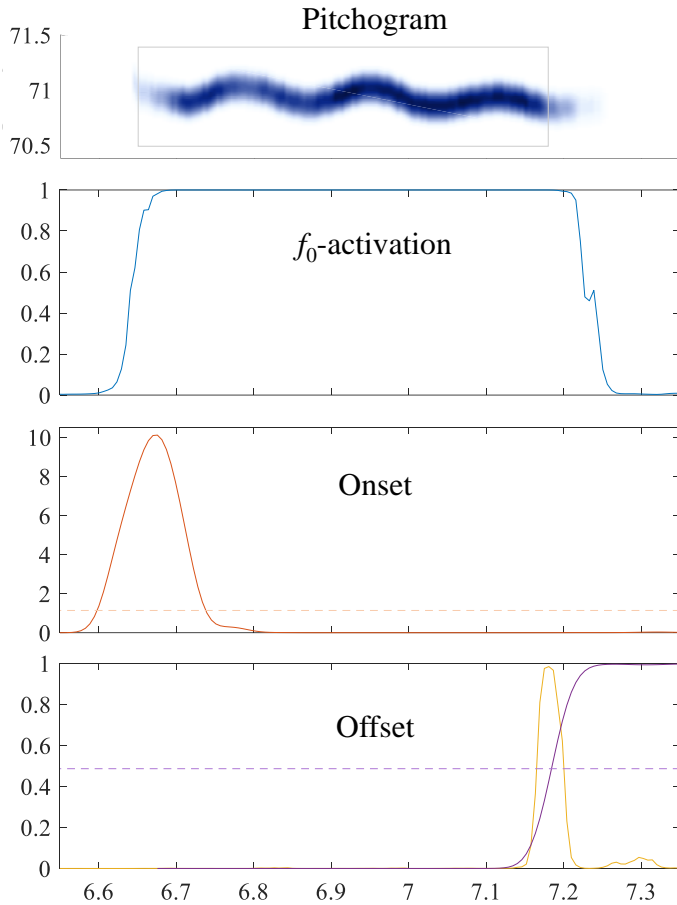


Figure 13. The Pitchogram representation of a note in polyphonic audio (Me No 2 of Bach10) with the note annotation (grey box), its f_0 -activation after the sigmoid activation function (blue line), and activation function for onsets and offsets. This is the same note that the pitch ridge was illustrated for in Figure 11. The onset activation (red line) is the *OCS* prior to thresholding at 1.2. The offset activation, *OFC* (yellow line), is shown together with the smoothed offset detection activation (purple line), prior to thresholding at 0.47 (purple dashed line).

By including the accumulated mean and sum of the representations at each frame, the network is provided with information of the characteristics of the note so far, in relation to the present state. The accumulated *OFC* will be higher if any changes in the spectrum indicative of an offset have occurred previously, while other accumulated activations and magnitudes provide more context regarding changes in the spectral characteristics and polyphonic texture.

To determine the final offset position, the output activations were smoothed across time with a Gaussian window ($\sigma = 4.3$), and the first time-frame with an activation $t > 0.47$ was chosen as the offset. These two parameters (σ and t) minimized the absolute distance to the annotated offset in a grid search across the training set. Shown in Figure 13 is the Pitchogram representation, and the f_0 , onset, and offset activations for a note played by the violin with vibrato in an excerpt of the four-voiced Bach10 dataset.

10. Note classification

Finally, notes were processed by the note classification neural network (N_6), and each note assigned a probability of being correct. The input features focused on context, while also providing information about the region, notes, and onsets.

10.1 Input features

Onsets

Given that the onset network was trained mostly based on the change of activation/signal level, and that this information, therefore, should be encoded in the resulting *OC*, the input to the note network instead mostly consisted of raw activations/signal levels. By the same reasoning (variation in input), the time indexing of T_4 was shifted two frames forward to be $\{-10 -6 -2 2 6 10\}$ (T_{4*}). The following information from the onset of the note was used for the input layer:

- The previously computed *OC* indexed at T_2 . The raw output from the network was used (prior to the sigmoid activation, thresholding, and smoothing), in order to retain as much information as possible for the note network.
- The last hidden layer of the onset network was included, indexed at T_{4*} .
- The input to the pitch network at the nearest Tentogram bin relative to the ridge frequency, indexed at T_{4*} .
- The signal level of L_{+25} , indexed at relative frequencies F_1 and times T_4 .
- The flux of the *LV* (specified in Section 5.3), but instead using relative frames between -15 and 15 with a step size of 3.

Note

Order statistics in the form of quintiles $\{25\ 50\ 75\}$, were collected for activations and signal levels across the length of the note for: the PF, the absolute PF, the *OC*, the *OCS*, the activations of the pitch network at the output layer and last hidden layer, and the 50 input features from L^4 to the tentogram network collected at the frequency index closest to the ridge pitch.

Context

Input features were computed based on the relationships between each note and adjacent notes extracted from the same region. These features included:

- The duration, inter-onset interval (IOI) and inter-pitch interval (IPI) of the evaluated note, the two previous notes, and two subsequent notes. If surrounding notes did not exist in the region, the duration was set to two seconds, the IOI to 3 seconds, and IPI to 0. The last note of the region was assigned an IOI one second longer than its duration, and an IPI of 0.
- The order of the evaluated note in the region, as well as the number of notes extracted from the region, were included as two additional features.

Furthermore, the onset activation of close onsets was collected, by summing the activations at each semitone relative to the evaluated note at ± 25 semitones (2 octaves and a semitone). The activations were summed within five time-ranges relative to the onset of the processed note $\{-18$ to -11 , -10 to -4 , -3 to 3 , 4 to 10 , 11 to $18\}$.

10.2 Run-time operation

During run-time (after training the network), notes were removed iteratively, in ascending order according to their computed probability of being correct. During this process, after each note-removal, the input features and note probabilities of surrounding notes affected by the presence of the removed note were updated. This included a new calculation of the offset for any note directly preceding the removed note in the same region. The procedure lessens the burden on the network to approximate the salience of other notes in close proximity, by always providing an accurate context of likely notes. For example, when a note *A* at an octave relation to another note *B* has been removed, the network may attribute harmonics in the spectrogram more clearly to note *B*, resulting in a higher probability. As another example, when a more accurate offset has been determined for a note after another onset that previously shortened the note has been removed, it can be expected that note features computed across its duration also become more accurate. The threshold for when to stop the note removal was set to 0.55, determined by testing $\{0.5 \rightarrow 0.6 \rightarrow 0.55\}$ in a small grid search on the training set.

10.3 Training

Training was done in two steps. In both steps, a set of training examples (Tr) was created for each ME in the training and validation set, and the network trained to classify each example as a correct or incorrect note. First, the system was run up until the note-removal step for each ME and all extracted tentative notes evaluated with the evaluation procedure described in Section 2.3, creating Tr . The note network was then trained with the extracted notes as training examples. In the second step, the system was run through the note-removal step by using the network trained during the first step. Both the kept and removed notes were gathered as tentative training examples Tr_T ; the removed notes had the input features extracted at the time of their removal in the first step. The note evaluation was performed on Tr_T , and the note that had been removed first during run-time was added to

the empty set Tr , and removed from Tr_T . This procedure was repeated for all notes removed during run-time. If a removed note was evaluated as true, the evaluation of notes in close proximity (pitch and time) was re-done, as the removal could have altered their evaluation from false to true due to the ordered structure of the evaluation procedure (Section 2.3). Finally, the notes kept during run-time were also added to Tr , using their assigned evaluation.

10.4 Shifting onsets and framewise F-measure - \mathcal{F}_{fr}

During the synthetization and annotation of the training set, the onset time of annotations was shifted forward based on the shape and length of the attack (envelope) of the instrument. This should generally result in worse performance for test sets where the music and annotations also are generated from MIDI, as the onset times will be transcribed later than the MIDI annotations on average. To account for this, the predicted note onset times were shifted 0.01 s earlier after the note classification step.

A framewise f_0 estimate was generated from the transcribed notes. The f_0 -predictions were defined as the time-varying pitch for each note (along the ridge), for all time-frames between the onset and the offset. Then, the combined predictions for each time-frame were analyzed. For all framewise predictions within 60 cents, the prediction with the highest f_0 -activation was kept and the other predictions removed. One reason for doing this is that notes may sometimes overlap without being assigned to the same region, for example during repeated notes of the same pitch with vibrato. Applying the evaluation procedure described in Section 2.3 for the predictions gave the framewise estimate \mathcal{F}_{fr} . This method gave slightly better framewise predictions than the \mathcal{F}_{frt} metric described in Section 7.2.

11. Regularization and Training performance

11.1 Regularization

When using the same training set for each step of the deep layered learning processes, the system will become over-reliant on the activations extracted from previous layers. It will appear as if the extracted activations are very predictive for the next step, when, in fact, information provided from skip connections may be more useful. The reason for this is the potential for overfitting, that will increase at every learning step of the system. In deep learning, drop-out can be used for regularization. This can also be used in each network for deep layered learning, but the iterative training also facilitates other methods. For example, in deep layered learning, the training set could be divided into smaller subsets, so that the different sets do not overfit in the same way. Another technique for regularization is to distort the training examples for each learning step of the deep layered system. This was the technique used for the present system. A very simple solution was used, only varying the frequency response of the initial spectrograms M for all tracks in the training set.

Each time-frame of M was filtered by multiplication by a vector F_M , spanning the 518 frequency bins. This vector was derived from the equivalent decibel scale vector F , which was created by summing smooth filters. First, ten Hann windows were used. The width w of each window was computed by using the uniform random discrete distribution U_d between odd integers from 1 to 241

$$w \sim U_d([1, 3, 5, \dots, 241]) + 120, \quad (21)$$

and the center c of the window across F was randomly selected from 518 potential integer values

$$c \sim U_d([1 - 518]). \quad (22)$$

The uniform random distribution U was used to select the amplitude a of each window as a floating-point number between -7 and 7,

$$a \sim U([-7 - 7]). \quad (23)$$

The Hann windows designed with the parameters in Eqs. 21-23 were summed to F , ignoring any parts of a window that fell outside the boundaries of the vector. A shelf window was then added with amplitude drawn from

$$U([-3.5, 3.5]), \quad (24)$$

and a center c determined by applying Eq. 22. The shelf fell or rose to 0 from the determined amplitude linearly over 60 bins, centered at c derived from Eq. 22. Shown in Figure 14 are four filters, all derived through Eqs. 21-24.

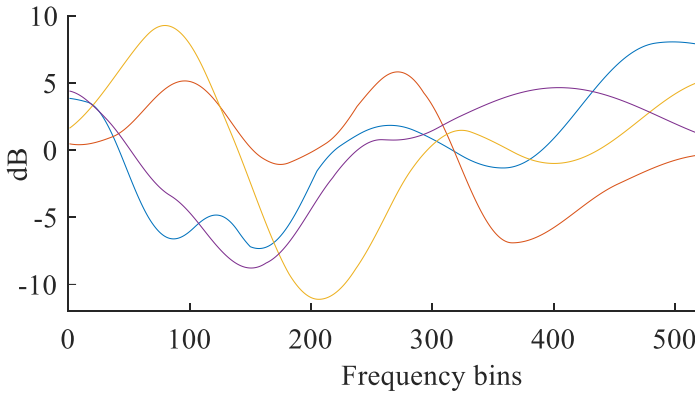


Figure 14. Four frequency filters used for regularization.

Finally, the multiplicative filter F_M was derived by subtracting the mean¹⁰ from F , and converting from the log-domain

¹⁰ Due to the normalization described in Section 5, the mean subtraction had no effect. This fact was not realized until after the evaluation.

$$F_M = 10^{\frac{F-\bar{F}}{20}}. \quad (25)$$

The regularization technique was used from the onset detection step, applied to M for all subsequent training iterations. During testing, it was not used. The regularization technique was added after first having run the complete training and testing without it, thereby providing an informal test of its effect. After training with regularization, \mathcal{F} decreased by around 0.5 for the training set and increased by around 1 for the test sets.

11.2 Training performance

The performance at each step of processing is provided for the training sets, to give an insight into, for example, how the \mathcal{R}/\mathcal{P} -balance varied during transcription and the amount of overfitting during training in relation to the test sets. Table 5 shows the results for the *Attacked* dataset, and Table 6 for the *Sustained* dataset. As shown, \mathcal{R} is kept high initially, to retain as much relevant information as possible. It then falls slightly at each step while pruning away false examples and increasing \mathcal{P} . After the final note classification, \mathcal{R} and \mathcal{P} are about the same. The low threshold used for the Tentogram allows for 80 % of the estimates to be incorrect but ensures a high framewise \mathcal{R} . The low threshold also ensures that pixels in the Tentogram and Pitchogram activate in the vicinity of well over 99 % of the annotated onsets.

	\mathcal{F}_{fr}	\mathcal{P}	\mathcal{R}	$\mathcal{F}_{on/off}$	\mathcal{P}	\mathcal{R}
Tentogram	28.3	16.7	94.0	-	-	99.7
Pitchogram	63.0	48.8	88.8	-	-	99.4
\mathcal{F}_{frt}	75.7	79.5	72.3	-	-	-
Onset	-	-	-	67.9	51.9	98.1
Note	88.9	94.1	84.2	96.4	98.1	94.6
Offset	-	-	-	86.7	88.3	85.2

Table 5. The performance progression for the *Attacked* dataset during training. A special version of \mathcal{R} is measured for onsets in the Tentogram and Pitchogram; the proportion of onset annotations that are within 50 cents and 120 ms of an activated f_0 . The framewise performance when using the threshold that maximizes \mathcal{F}_{fr} is provided as \mathcal{F}_{frt} . The framewise performance determined from using the frames between onset and offset of notes is provided in the *Note* column.

	\mathcal{F}_{fr}	\mathcal{P}	\mathcal{R}	$\mathcal{F}_{on/off}$	\mathcal{P}	\mathcal{R}
Tentogram	28.5	16.7	97.5	-	-	99.9
Pitchogram	81.0	69.7	96.7	-	-	99.8
\mathcal{F}_{frt}	88.4	86.0	90.9	-	-	-
Onset	-	-	-	78.7	65.9	97.7
Note	95.6	96.6	94.6	97.1	98.2	96.0
Offset	-	-	-	93.8	94.9	92.7

Table 6. The performance progression for the *Sustained* dataset during training. See the text for Table 5 for an overview.

12. Evaluation

12.1 Main results

Table 7 shows the framewise performance for the test sets and Table 8 shows the note-based performance. The onset-offset pitch ridge (Section 10.4) was used for the framewise estimate; it increased \mathcal{F}_{fr} by between 0-5 on the training and test sets in comparison with the thresholded Pitchogram estimate (Section 7.2).

Test Set	A_{fr}	\mathcal{F}_{fr}	\mathcal{P}	\mathcal{R}
Bach10	85.6	92.2	91.4	93.1
MAPS	64.5	78.4	84.9	72.8
TRIOS	56.0	71.8	91.1	59.2
Woodwind	57.4	72.9	74.7	71.2

Table 7. The framewise performance of the system for the four test sets.

Test Set	A_{on}	\mathcal{F}_{on}	\mathcal{P}	\mathcal{R}	\mathcal{F}_{off}	\mathcal{P}	\mathcal{R}	\mathcal{F}_{off}^{on}	\mathcal{P}	\mathcal{R}
Bach10	79.0	88.3	87.0	89.6	88.0	86.7	89.3	84.2	83.0	85.4
MAPS	82.4	90.3	91.4	89.3	70.1	71.0	69.3	58.0	58.7	57.3
TRIOS	72.1	83.8	85.8	81.8	47.0	48.2	45.9	39.1	40.0	38.1
Woodwind	68.9	81.6	87.7	76.3	75.8	81.5	70.8	51.1	54.9	47.8

Table 8. The note-based performance of the system for the four test sets.

There seems to be a difference in performance for datasets where the system had seen similar types of examples (Bach10 and MAPS) and for datasets where no similar examples were present (TRIOS and Woodwind). The system, however, achieves high results for these unfamiliar examples as well. Offsets are harder to estimate than onsets for the system, which can be expected as these are less defined for hammered instruments. However, for datasets only containing sustained instruments (Bach10 and Woodwind), the performance is almost equal (differing measurement windows unaccounted for).

The onset annotations for the Disklavier pianos of the MAPS dataset and the Bach10 dataset have a rather inaccurate timing, which leads to correct estimates being classified as incorrect. Performance measures with an 80 ms window are therefore also provided in Table 9 for future reference.

80 ms	\mathcal{F}_{on}	\mathcal{P}	\mathcal{R}
MAPS	91.4	92.5	90.4
Bach10	91.9	90.6	93.3

Table 9. Performance when allowing a distance of 80 ms for onsets.

12.2 Comparison overview

More detailed performance and comparison with other systems are presented in the following subsections for each dataset. Several previous systems have been evaluated on the datasets. The systems used for comparison are listed in Table 10. As other publications

often use a 50 ms window for onset tracking, this was the window used when comparing with other systems.

Abbr.	Short description & Reference	Eval.	Sets
Ben13	Explicit duration HMM (Benetos & Weyde, 2013)		MWT
Ben13b	Efficient shift-inv. PLCA (Benetos et al., 2013)	Su15 _B	BMWT
Ben15	Constrained PLCA (Benetos & Weyde, 2015)	Pes17 _{M+}	BMWT
BL12	Musical model-RNN on top of a classifier (Boulanger-Lewandowski et al., 2012)	Pes17 _{M+}	M+
Dres17	Rule-based bottom-up approach (Dressler, 2017)	Prop. _{BMWT}	BMWT
Duan10	Analyzing spectral peak and non-peak regions (Duan et al., 2010)		B
Haw17	CNN + bidirectional LSTM (Hawthorne et al., 2017)		M+
Kir14	Unsupervised spectral modeling initialized with isolated MAPS data (Berg-Kirkpatrick et al. 2014)		M
Klap06	Summing harmonic amplitudes (Klapuri, 2006)	Duan10 _B ; Pes17 _M	BM+
Klap08	Auditory model and periodicity analysis (Klapuri, 2008)	Peel11 _w	W
Kelz16	CNN with octave-sized kernels (Kelz et al., 2016)	Haw17 _{M+}	M+
Nak18	ERB - PLCA (Nakamura et al., 2018)		M
Peel11	Maximum-likelihood over Poisson process (Peeling & Godsill, 2011)		W
Pert08	Spectral peak analysis (Pertusa & Iñesta, 2008)	Duan10 _B	B
Pes17	Unsupervised layerwise learning (Pesek et al., 2017)		M+
Sch17	PLCA + frame-level classifier using a few spectral features (Schramm & Benetos, 2017)		B
Sig14	RNN trained with templates of B (Sigtia et al., 2014)		B
Sig16	CNN with local receptive fields (Sigtia et al., 2016)	Haw17 _{M+}	M+
SONIC	Oscillator and note networks for piano (Marolt, 2004)	Su15 _{BMT}	BMT
Su15	Partial analysis and modeling (Su & Yang, 2015)		BMT
Vinc10	NMF-like decomposition (Vincent et al., 2010)	Kir14 _{Mon} ; Su15 _{BT}	BMTW*

Table 10. Overview of systems used for performance comparison and their abbreviations (*Abbr.*). A *Short description* is offered, and the publication providing the *Evaluation* is marked if it was collected from outside of the *Reference* for the system. The *Evaluation* is provided in the form $\text{Abbr}_{\text{Datasets}}$, and *Datasets* is encoded by {B = Bach10, M = first 30 seconds of all tracks in MAPS ENSTDkCl, M+ = complete or larger part of MAPS dataset, W = Woodwind quintet, T = the TRIOS dataset}.

Additionally tested system

Dressler (2017) was kind enough to run the Dres17 system on the four test sets and provide its output. The evaluation of onset and offset tracking is shown in Table 11. As is evident, the proposed system outperforms Dres17 regarding offset tracking. The difference is smallest for the TRIOS and Woodwind datasets. Onset tracking is compared together with the rest of the systems in Sections 12.3-6.

	\mathcal{F}_{on}	\mathcal{P}	\mathcal{R}	\mathcal{F}_{off}	\mathcal{P}	\mathcal{R}
Bach10	63.0	62.8	63.1	61.0	60.9	61.2
MAPS	55.1	65.4	47.6	29.1	34.6	25.2
TRIOS	55.4	63.1	49.4	42.8	48.7	38.1
Woodwind	63.9	77.0	54.6	67.4	81.1	57.6

Table 11. Results for Dres17 for pitched onset and offset tracking across the four test sets.

For all figures, the orange and white bars represent the main metric, light blue ticks represent \mathcal{R} , and dark green ticks \mathcal{P} . If ticks are omitted, \mathcal{R} and \mathcal{P} were not provided in the evaluation.

12.3 Bach10

The performance comparison on Bach10 for note tracking is presented in Figure 15, and for f_0 -estimation in Figure 16 (\mathcal{F}_{fr}) and Figure 17 (A_{fr}). The proposed system clearly outperforms other systems for both tasks. For note tracking, the error-rate ($1 - \mathcal{F}_{on}$) is reduced from 34.84 to 11.7 in comparison with the best previous system, corresponding to a reduction of errors by a factor of three. The reduction is probably even higher than this, as discussed in Section 13.2.

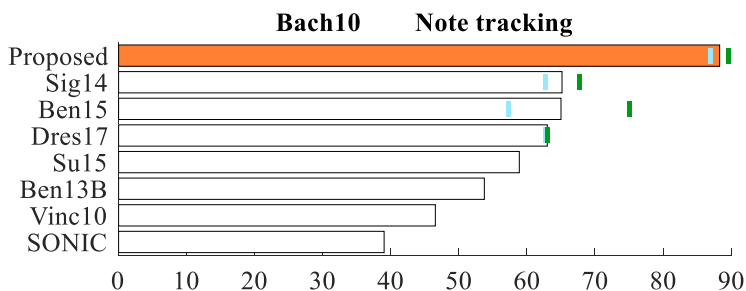


Figure 15. Comparing \mathcal{F}_{on} for Bach10. Dark green represents \mathcal{R} and light blue \mathcal{P} .

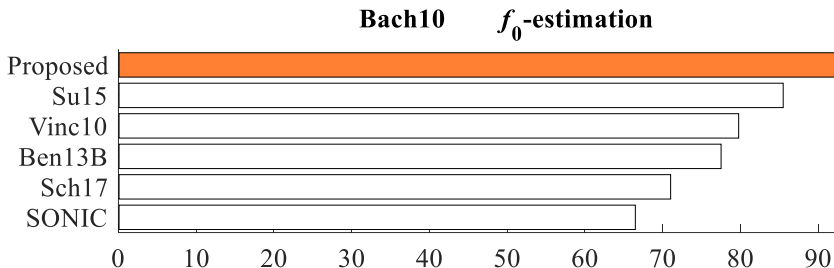


Figure 16. Comparing \mathcal{F}_{fr} for Bach10.

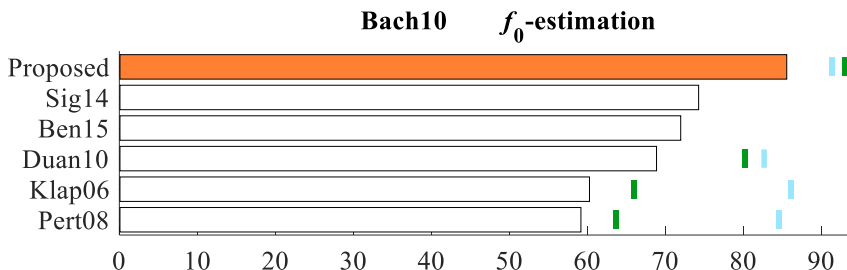


Figure 17. Comparing A_{fr} on the Bach10 dataset for systems that did not have \mathcal{F}_{fr} computed.

For Sig14, the best out of nine evaluated configurations in the study is used. The method uses an RNN trained with pre-extracted and pre-shifted spectral templates of the specific instruments present in the Bach10 dataset. A grid search across parameters was used for Vinc10, Ben13B, and Su15 to optimize Bach10 test performance (Su & Yang, 2015). SONIC was trained for piano which could explain the low performance. Two systems were developed before the test set was released, Klap06 and Pert08. Note that differences can incorrectly be perceived as bigger with A_{fr} than \mathcal{F}_{fr} as the former metric “counts errors twice” (see Eq. 5).

12.4 MAPS

Table 12 shows the framewise performance of the system for the MAPS dataset broken down into various subsets, and Table 13 shows the performance for onset and offset detection. For both tables, the first nine rows are the results broken down into the different pianos, and the last two rows are the combined performance for the Disklavier pianos and the 7 MIDI-pianos respectively. Many systems only compute performance statistics for the first 30 seconds of the tracks in ENSTDkCl, to save time/memory for resource-intensive systems. These results (ENSTDkCl30) are therefore used for comparison and highlighted in bold in the tables.

Subset	A_{fr}	\mathcal{F}_{fr}	\mathcal{P}	\mathcal{R}
AkPnBcht	69.2	81.8	87.6	76.7
AkPnBsdf	64.3	78.3	80.9	75.7
AkPnCGdD	69.5	82.0	85.7	78.7
AkPnStgb	60.6	75.5	83.7	68.7
ENSTDkAm	55.4	71.3	82.3	62.9
ENSTDkCl	59.3	74.4	85.8	65.8
SptkBGAm	66.6	80.0	86.4	74.4
SptkBGC1	68.1	81.0	86.5	76.2
StbgTGd2	70.1	82.5	85.7	79.4
ENSTDkCl30	61.0	75.8	84.7	68.5
MAPS D	57.4	72.9	84.1	64.4
MAPS MIDI	66.9	80.2	85.2	75.7

Table 12. Framewise performance on different subsets of the MAPS dataset. For D and MIDI, results were computed as the average on a subset basis, i.e., by averaging the results computed for each piano. The results for ENSTDkCl30 are used for comparison with other systems.

Subset	A_{on}	\mathcal{F}_{on}	\mathcal{P}	\mathcal{R}	\mathcal{F}_{off}	\mathcal{P}	\mathcal{R}	\mathcal{F}_{off}^{on}	\mathcal{P}	\mathcal{R}
AkPnBcht	91.1	95.3	97.2	93.5	72.7	74.2	71.3	68.8	70.2	67.5
AkPnBsdf	85.8	92.4	92.4	92.3	69.0	69.1	69.0	60.6	60.6	60.6
AkPnCGdD	88.0	93.6	95.9	91.5	74.5	76.3	72.8	68.7	70.3	67.1
AkPnStgb	85.4	92.1	90.7	93.6	69.3	68.2	70.4	62.8	61.8	63.8
ENSTDkAm	66.9	80.2	82.4	78.1	63.1	64.8	61.5	42.6	43.8	41.5
ENSTDkCl	74.9	85.6	87.5	83.8	66.1	67.5	64.7	51.4	52.5	50.3
SptkBGAm	85.4	92.1	91.7	92.5	67.1	66.8	67.5	53.5	53.3	53.8
SptkBGC1	86.3	92.6	93.6	91.7	74.3	75.1	73.5	59.8	60.5	59.2
StbgTGd2	85.6	92.2	94.7	90.0	76.8	78.8	74.9	58.0	59.5	56.6
ENSTDkCl30	77.5	87.3	87.4	87.2	67.6	67.6	67.5	51.4	52.5	50.3
MAPS D	70.9	82.9	85.0	81.0	64.6	66.2	63.1	47.0	48.2	45.9
MAPS MIDI	86.8	92.9	93.7	92.2	72.0	72.6	71.3	61.6	62.3	61.2

Table 13. Performance for onset and offset tracking on different subsets of the MAPS dataset. See the text for Table 12 for further details.

Performance is lower for the Disklavier recorded in an ambient setting (ENSTDkAm), and to some extent also for the closely recorded ENSTDkCl. This can partly be explained by the inaccuracy in timing for the annotations of these subsets; they are too early in relation to the sounds. A likely explanation is that the time for the sound to travel from the piano to the microphones is unaccounted for. The error seems to be a little less than 10 ms for ENSTDkCl and about 20 ms for ENSTDkAm. The annotations were therefore shifted according to these numbers (10 ms and 20 ms), and the Disklavier pianos evaluated again for the onset-related metrics \mathcal{F}_{on} and \mathcal{F}_{off}^{on} as shown in Table 14. These results were not used in comparison with other systems. It can, however, be expected that the

systems both trained and tested on these MAPS subsets implicitly compensate for the shift. Furthermore, the systems that *only* evaluate on the Disklavier subsets may have explicitly or implicitly compensated for the shifted annotations (e.g., through parameter tuning, where parameters affect onset times).

Test Set	A_{on}	\mathcal{F}_{on}	\mathcal{P}	\mathcal{R}	\mathcal{F}_{off}^{on}	\mathcal{P}	\mathcal{R}
ENSTDkAm	70.1	82.5	84.7	80.3	47.8	49.1	46.5
ENSTDkCl	74.8	85.6	87.5	83.8	52.1	53.2	51.0
MAPS D	72.5	84.1	86.1	82.1	50.0	51.2	48.8

Table 14. Performance for onset and offset tracking on different subsets of the MAPS dataset when compensating for timing errors in the annotations.

A comparison with the systems that have been evaluated for \mathcal{F}_{on} on the MAPS ENSTDkCl dataset is shown in Figure 18. The proposed system outperforms other systems for the task. Systems specifically designed for piano transcription (Haw17, SONIC, Kir14, Nak18) generally have the highest results among the comparison systems. Many systems were trained with overlapping compositions (using the same MIDI performance) in the training and test set. This may result in overfitting – recent research suggests that deep neural networks with similar architectures (e.g., Kelz16) have problems generalizing to unseen combinations of notes (Kelz & Widmer, 2017). A grid-search across parameters was performed for many systems, to find the parameters that maximized test performance.

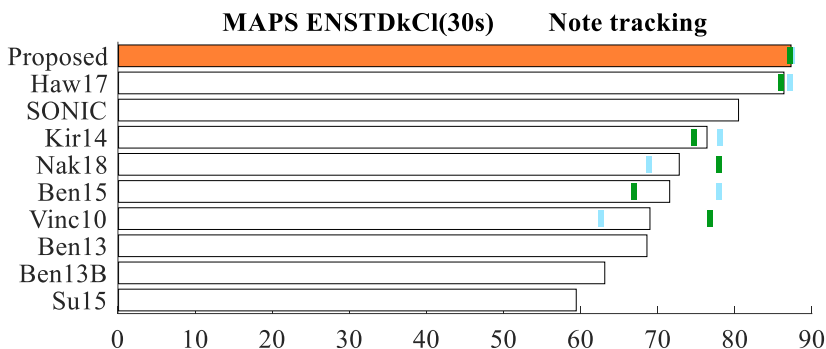


Figure 18. Comparing \mathcal{F}_{on} for the MAPS ENSTDkCl dataset, using the first 30 seconds of each track. Dark green represents \mathcal{R} and light blue \mathcal{P} .

Omitted are systems by O’Hanlon and Plumbley (2014), Cheng et al. (2016), and Gao et al. (2017) with a relatively high performance for note tracking ($\mathcal{F}_{on} = 58.3, 82.36,$ and 85.06 respectively). These were trained exclusively with isolated piano samples from the ENSTDkCl piano, the same subset that they were evaluated for. Such a methodology can overfit the data to such an extent that it is hard to draw conclusions about performance. By comparison, the proposed system had $\mathcal{F}_{on} = 96.4$ on the validation set used in this study during training. Of course, the systems trained only on piano sounds, especially with overlapping compositions and performances between training and test set, may also

overfit rather substantially (certainly if piano transcription is regarded as a special case of polyphonic transcription).

Shown in Figure 19 is a comparison with previous systems for f_0 -estimation. It can be noted that f_0 -estimation is hard for hammered instruments (such as the piano), because it is not always clear when the notes end.

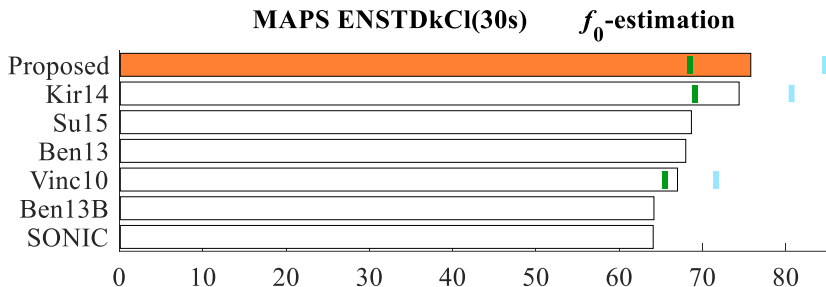


Figure 19. Comparing \mathcal{F}_{fr} for the MAPS ENSTDkCl dataset, using the first 30 seconds of each track.

SONIC, which had the highest \mathcal{F}_{on} among the systems included for comparison, also had the lowest \mathcal{F}_{fr} . This system, therefore, seems to have a hard time estimating offsets.

Table 15 shows results for comparison-systems that were evaluated across the two Disklavier subsets (D), or the rest of the subsets (MIDI). The D-subset is commonly used by machine learning systems focused on piano transcription, training the system on the MIDI subset although some of the compositions are overlapping. Some systems remove overlapping compositions (Haw17), whereas others apparently do not (Kelz16, and Sig16). The results reported for the proposed system (Tables 12-14) are competitive with the best performing system Haw17 for the combined Disklavier set (D), and outperform systems tested for the MIDI set.

Subset	D			MIDI
	\mathcal{F}_{fr}	\mathcal{F}_{on}	\mathcal{F}_{off}^{on}	\mathcal{F}_{fr}
Ben15	56.7	-	-	62.6
BL12	57.1	-	-	61.6
Haw17	78.3	82.3	50.2	-
Kelz16	70.6	50.9	23.1	-
Klap06	52.5	-	-	56.0
Pes17	51.8	-	-	52.6
Sig16	64.1	54.89	18.4	-

Table 15. Performance metrics \mathcal{F}_{fr} , \mathcal{F}_{on} , and \mathcal{F}_{off}^{on} for comparison systems evaluated on the Disklavier subsets, as well as \mathcal{F}_{fr} across the MIDI subsets.

12.5 TRIOS

Shown in Figure 20 is the performance of the evaluated algorithms for note tracking on the TRIOS dataset. The proposed system clearly outperforms other algorithms, and the error rate is more than halved in comparison with the previous state-of-the-art. The results are encouraging when considering that the system did not train on any tracks with a mix of sustained instruments and piano. Performance for the track “Take Five” that contains drums is not degraded ($\mathcal{F} = 90.7$, $\mathcal{P} = 88.7$, $\mathcal{R} = 92.9$). This indicates that the system can be used for note detection in regular music mixes with drums.

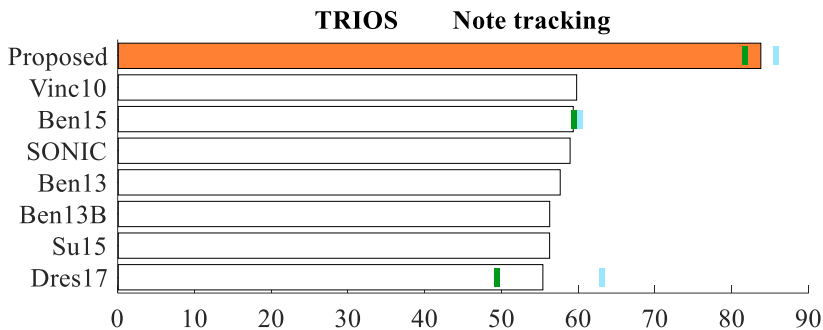


Figure 20. Comparing \mathcal{F}_{on} for the TRIOS dataset. Dark green lines represent \mathcal{R} and light blue lines \mathcal{P} .

Figure 21 shows the performance for f_0 estimation. The system has never analyzed a mix of hammered and sustained instruments during training and struggles to detect off-sets, as indicated in Table 8. Many offsets are cut short, which reduces \mathcal{R} for f_0 estimation. The system, therefore, only barely performs a new state-of-the-art.

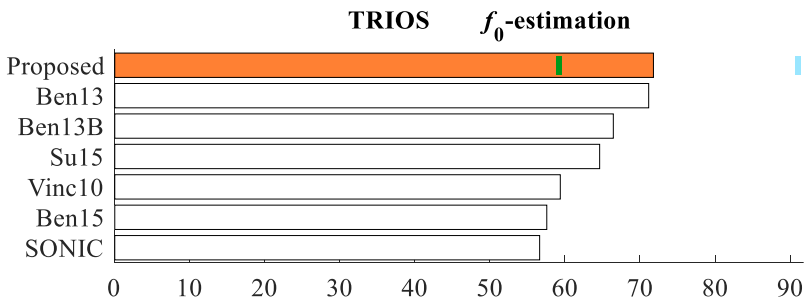


Figure 21. Comparing \mathcal{F}_{fr} for the TRIOS dataset. Dark green lines represent \mathcal{R} and light blue lines \mathcal{P} .

12.6 Woodwind

Shown in Figure 22 is a comparison of note tracking performance on the Woodwind data. All comparison systems use PLCA-type methodologies. The music track contains five voices and many tones with staccato. Neither of these features is present in the training

set of sustained instruments. Nevertheless, the proposed system has a clearly higher performance than the other systems.

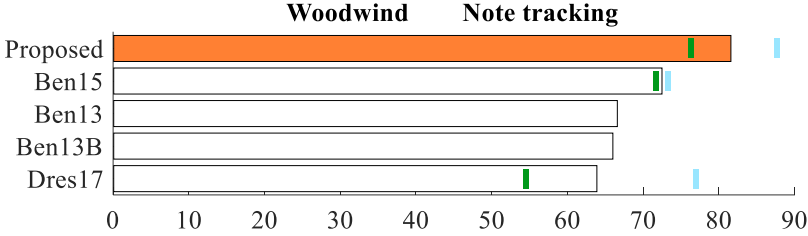


Figure 22. Comparing \mathcal{F}_{on} for the MIREX Woodwind test set. Dark green lines represent \mathcal{R} and light blue lines \mathcal{P} .

Presented in Figure 23 is the f_0 -estimation performance of the compared systems on the Woodwind data. The proposed system clearly outperforms other systems. Performance should rise if some similar music tracks are added to the training set.

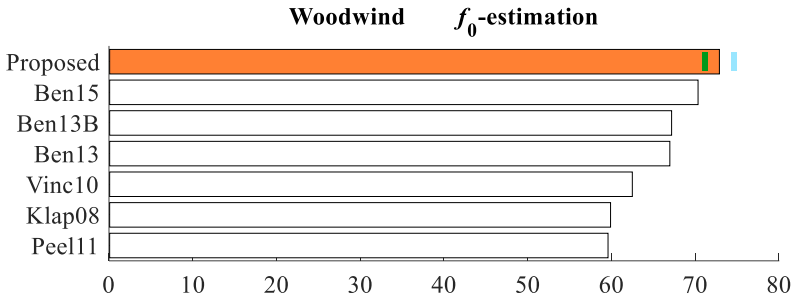


Figure 23. Comparing \mathcal{F}_{fr} for the Woodwind test set.

12.7 Combined metric

The datasets cover a rather wide range of polyphonic music (although more modern examples would also be useful). How can the performance of the systems be measured across the test sets? A simple method would be to compute a combined \mathcal{F} for the four datasets, as their harmonic mean. This combined metric, $\bar{\mathcal{F}}$, is computed as

$$\bar{\mathcal{F}} = \frac{4}{1/\mathcal{F}_{\text{Bach10}} + 1/\mathcal{F}_{\text{MAPS}} + 1/\mathcal{F}_{\text{Trios}} + 1/\mathcal{F}_{\text{Woodwind}}}. \quad (26)$$

The combined results for the proposed systems using the numbers reported in Tables 7-8 are presented in Table 17. The table also includes results for Dres17.

Bach10, MAPS, TRIOS, Woodwind				
	<i>fr</i>	<i>on</i>	<i>off</i>	<i>on+off</i>
Proposed	78.1	85.9	66.6	53.9
Dres17	-	59.1	45.0	-

Table 17. Results using the combined metric \bar{F} for evaluating the test sets.

The most common combination of evaluated test sets is BMT, as defined in Table 10 (using the ENSTDkCl subset). Therefore, combined results across these sets are provided in Table 18.

Bach10, MAPS ENSTDkCl, TRIOS				
	<i>fr</i>	<i>on</i>	<i>off</i>	<i>on+off</i>
Proposed	79.0	88.4	63.2	52.7
SONIC	54.6	62.1	-	-
Vinc10	56.9	67.7	-	-
Su15	58.2	71.9	-	-
Ben13b	57.5	68.9	-	-
Ben15	-	64.9	-	-

Table 18. Results using a combined metric \bar{F} for evaluating the Bach10, MAPS ENSTDkCl30, and TRIOS test sets.

The comparison in Section 12.2-7 has shown that the proposed system sets a new state-of-the-art for polyphonic pitch tracking. The system is especially good at tracking onsets and can perform across a wide range of instrumentations. The variation in performance on different test sets for the systems motivates the use of the proposed combined \bar{F} in future publications. Machine learning systems trained only on piano examples seem to struggle for other datasets (or do not report results at all). It is striking that the comparison systems in Table 18 are so similar in performance when three test sets are used. The system by Su and Yang (2015) however seems to be the second strongest overall.

13. Conclusions, Discussion, and Future work

13.1 Contributions

This article has suggested a few interesting processing strategies for polyphonic pitch tracking, including:

- A simple processing strategy for spectrogram whitening and normalization that can be performed in a time-casual manner.
- A method for processing a music spectrogram with a sparse convolutional kernel, where the relative frequencies of bins that are used and that utilize weight sharing have been learned beforehand.

- A method for pruning and upsampling the search space by computing tentative f_0 s in a Tentogram:
 - using a linear combination of spectrogram bin levels and DCT components that describe a desirable response across pitch.
 - Combining parameters by summing shifted spectrograms, a constant, and the computed pitch response vector. The tentative f_0 s were then detected by peak-picking in the thresholded spectrogram and upsampled with parabolic interpolation.
 - Cascading a second step for f_0 estimation that is applied only to the most likely pitches in each frame, using a bigger network and including activations from the first step as input.
- A method for tracking tones across time and pitch to extract pitch ridges.
- A method for pruning the search space for onsets and offsets, by only processing time-frequency positions in the proximity of identified f_0 s.
- A method for extracting the neural flux for note tracking by training a network to make a framewise f_0 -estimation, and then computing the change in latent representations of this network across time.
- A method for computing activations for pitched onsets and offsets by:
 - letting identified pitch ridges form a structural framework, so that spectral properties and latent representations of earlier networks can be captured with high precision relative to local pitch;
 - thereby enabling a neural network layer to convolve the pitch ridge using tone-shift-invariant input features;
 - as a result, developing a network that can process steady and fluctuating tones with the same neural weights, to the extent that it is perceptually accurate to do so, i.e.:
 - a tone-shift-invariant onset and offset activation network.
- A method for computing an offset probability function by using a network that receives cumulative information from spectral and latent representations across the length of the pitch ridge, thereby reducing the risk of detecting offsets:
 - early, from spurious offset activations, e.g., reacting to spurious decreases in energy in the tone;
 - late, as cumulative input features can provide adequate information for, e.g., tones with slowly decreasing energy, or tones with irregularly decreasing energy in steps that are too small by themselves to indicate an offset.
- A method for extracting as accurate information as possible when removing spurious notes by:
 - using not only accurate onsets but also accurate offsets for the notes, and with the aid of these;
 - extracting order statistics of spectral and latent representations across an accurate pitch ridge of the notes;
 - extracting contextual information of neighboring notes with an accuracy that increases throughout processing by;

- iteratively removing the notes most likely to be incorrect, while updating contextual information for all surrounding notes.
- A simple regularization technique for layered learning systems involving randomized equalization of the spectrogram at each learning step (with suggested expansions in Section 13.4)

Furthermore, strategies were suggested for:

- evaluating pitch tracking estimates ordered according to the distance from annotations, thereby avoiding mismatched pairings;
- automatically creating a large training set from MIDI data.

A new error metric was also proposed that combines the results from four test sets, and a larger evaluation of earlier pitch tracking systems provided.

13.2 Performance

Given that the system has the highest performance on four different datasets, concerning both \mathcal{F}_{fr} and \mathcal{F}_{on} , we conclude that it represents a new state-of-the-art in polyphonic pitch tracking. The system also had a high performance for offset detection in comparison with other competitive systems. However, data for offset detection are scarce; other systems have not been as focused on detecting (and evaluating) offsets as onsets. The performance for onset detection and offset detection in systems that perform note tracking will likely covary – an incorrect note will produce errors for both measures. Arguably, it would be more meaningful to measure and visualize performance as $100 - \mathcal{F}$ rather than to use \mathcal{F} . Improving \mathcal{F} from 90 to 95 is perceptually more meaningful than when the performance is improved from 75 to 80. This is better illustrated when showing how far from a perfect performance the system is, relative to others. Figure 24 shows the performance for onset detection on the Bach10 set as $100 - \mathcal{F}$. This way of illustrating performance more clearly shows that the proposed system reduces the number of errors by a factor of three in comparison with the previous state-of-the-art.

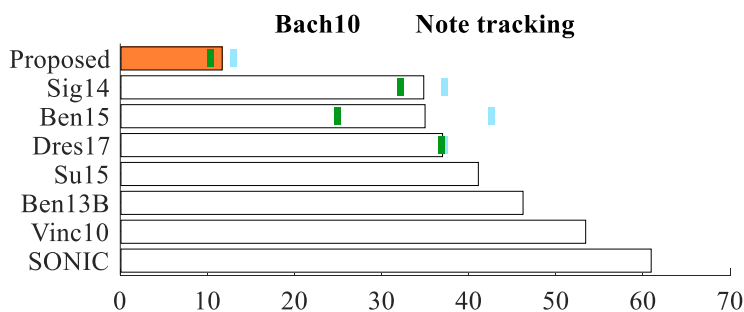


Figure 24. Note tracking performance for the Bach10 dataset displayed as $100 - \mathcal{F}_{on}$. As shown, the system significantly reduces the errors in relation to previous systems.

As previously stated, a fair number of onsets in Bach10 are annotated with an incorrect timing (they were annotated automatically with a system not specifically trained for

detecting onsets). As shown in Table 9, when a distance of 80 ms is allowed during evaluation, \mathcal{F}_{on} rises from 88.3 to 91.9. When allowing a 200 ms distance, \mathcal{F}_{on} becomes 93.6. A manual inspection by the author suggests that the difference can mainly be attributed to incorrectly timed annotations. The dataset also consists of many notes with overlapping onsets, i.e., two onsets by different instruments with the same pitch and onset time. It is very hard to detect and estimate these as two separate onsets. Furthermore, as noted by Miron et al. (2014), repeating notes are sometimes annotated by a single note (due to mistakes in the automatic annotation). In conclusion, optimal $1 - \mathcal{F}$ on the Bach10 dataset with the present annotations is not 0, but rather, closer to 5.0. This suggests that the part of the error which *can* be reduced *was* reduced by a factor of 4-5.

In the evaluation of the proposed system, there are large differences in performance between the validation sets (Tables 5-6) and the test sets. This discrepancy underlines how deceptive it can be to judge the performance of a system that has been trained and tested with the same kind of data (e.g., trained and tested with overlapping subsets of the MAPS dataset). Even though the training and validation sets are generated by 54 different GM instruments, which should give reasonable generalization, the difference compared to some of the test sets is very high. If the goal is to test the ability of an architecture to track polyphonic pitches, it seems reasonable to train and test over a variety of instruments. By limiting oneself to a specific instrument, especially for testing, it is impossible to know the extent to which a system generalizes in real-world applications. Methodologies that are “good” at overfitting to irrelevant confounding factors of variations, such as spectral characteristics, will be promoted. In this sense, the test sets that we use influence the direction of research. Therefore, it would be encouraging to see an adoption of the proposed test-score for a combination of test sets proposed in Eqs. 26-27 and evaluated in Tables 17-18.

13.3 Pruning strategies

Some observations can be made concerning the pruning strategies of the processing. The framewise f_0 s in the first learning step were computed from 50 linearly combined spectrogram bins, together with an additional weight vector accounting for the whitening and floor of the spectrum. This was done to obtain a simple initial estimate of present pitches, to which more advanced methods could be applied. Compared with cascading classifiers commonly used for pruning in the past (Viola and Jones, 2001), the initial number of parameters are rather high. For faster processing, the step could, therefore, be divided into several layers of classifiers with fewer parameters in each layer. For this pruning step, increased recall at the cost of a low precision is only negative to the extent that it slows down processing.

The next pruning step for computing the Pitchogram is, however, followed by the identification of regions and pitch ridges (Section 7.4). In this case, too low precision will serve to degrade the usefulness of the extracted regions. Spurious smaller regions can interfere during interpolation of the ridge pitch between larger regions (as shown in Figure 11), or, in dense mixtures with vibrato, connect regions one semitone apart. To improve the process, the extraction of connected regions and pitch ridges could be tuned

by adding an additional learning layer. Such a layer could label regions extracted during run-time as true or false, based on framewise (or onset-offset) annotations. From such labels, an algorithm for the pitch ridge extraction could be learned. Further details are beyond the scope of this article.

The note classification is pruned by extracting tentative notes from which further information is collected. Too low precision in tentative notes may degrade performance also here. Sometimes this can lead to spurious note onsets being extracted from the *OC* that interact with correct onsets in complex ways. For example, a spurious note onset just after a correct onset in the same ridge will initially be assigned a ridge all the way from the incorrect onset to the correct offset. Until the incorrect note is removed, the correct note will only consist of a short fragment with an offset at the spurious note onset. This situation highlights the importance of an iterative procedure for removing tentative notes, continually computing an updated context.

It may be interesting to estimate how pruning reduces the search space for note-tracking. Given a hop-size of 0.0058 seconds, 1563 pitch bins to explore, and 20 evaluated notes/s, the final search space for classification is reduced to less than $1/10000^{\text{th}}$ of its original size, $20 \times 0.0058 / 1563 = 0.000074$.

13.4 Regularization and training set

The equalization technique proposed for regularization is a fairly simple one. What other audio effects could be applied for regularization? Numerous audio degradation techniques for robust evaluation of MIR algorithms have been proposed by Mauch and Ewert (2013), some of which are used in the *evaluation* of various polyphonic transcription algorithms by Li and Su (2015). Many degradation techniques could be used for *regularization* as well. Useful degradations for the regularization of polyphonic transcription systems during training are listed below (a thorough description of the degradation techniques is, however, beyond the scope of this article). For all degradation techniques, it is assumed that the signal level of the ME has been normalized before degradation. Otherwise, the shape of the degradation will be systematically affected by the signal level of the MEs, which would introduce bias in the machine learning training.

Added sounds – Sounds can be added that do not alter the perception of pitch or the timing of onset and offsets in the recording. The spectrum of the *added* sound can be randomly and independently equalized. Three rough categories of sounds are:

- Adding random noise, e.g., white noise.
- Adding non-pitched sounds. This can include sounds that normally occur during musical recordings, such as squeaking chairs or pedaling noises. It could also be noises that may seem more artificial in a recording environment, such as rustling leaves or subway trains.
- Adding pitched sounds that are at such a low level or of such character that they will not be considered part of the performance. Such added noises are important if the system must be able to analyze polyphonic music in noisy settings. It can include voices, pitched nature sounds, and pitch artifact from instrumental performances.

Distortion – The audio signal can be distorted by clipping, soft clipping, saturation, or other forms of distortion regularly applied to music signal during production. Effects that add subharmonics, to the extent that the perception of f_0 s is altered, can however not be used.

Dynamic range processing – The dynamic range can be compressed or expanded with a compressor, expander, or limiter. Common processor settings can be varied randomly within reasonable ranges (e.g., attack 0-30 ms, release 100-500 ms, etc.). For compressors and limiters, the gain reduction must not be so extreme as to suppress perceived onsets (and thereby offsets) for repeated tones of the same pitch. For expanders, the audio expansion must not be so extreme that it gives rise to new perceived onsets (and thereby offsets) in sustained notes that vary in amplitude.

Reverbation – Different room acoustics can be added to the recording. Reverbation will shift the perceived onset and offset positions. Therefore, it has to be kept at a reasonable level. The pre-delay of the reverb should be kept low so as not to affect perceived onset times too much, and the decay of the reverb can also be kept low so as not to shift offset position too much.

Lossy audio compression – As proposed by Mauch and Ewert (2013), lossy audio data compression (e.g., MP3) can be applied to encode and then decode the signal. As these algorithms have been developed to retain perceptual qualities of the music, they should be suitable.

For all proposed degradation techniques, it is assumed that they are applied in a randomized fashion. Degradation processes should ideally be combined, with the amount of degradation, the order in which degradation techniques are applied, and the parameters during processing, all varied randomly for each track. It can be noted that many of the recent publications for polyphonic transcription would likely get a *reduced* performance from the above-proposed regularization techniques, as their test and training sets are so extensively overlapping.

The training set was synthesized from MIDI data. Some specific features of tone-starts were not captured well in the training set. Specifically, the training set did not contain onsets formed through portamento. However, overall, it seems that training sets created by the method described in this article were useful, given the high performance of the system. Regularization techniques such as those proposed are especially useful when the training set covers a small range of the variation generally found in music – as can be expected from MIDI-synthesized audio from a single SoundFont. Obviously, the randomness and added expressivity of real performances are beneficial for testing under real-world circumstances.

If the training set captured a larger range of the variation that exists in music performances (and that also exists in the test sets), the performance could be increased significantly. A straightforward way of increasing the variation of the training examples would, of course, be to vary the compositions and SoundFonts, or to use real instrumental performances. There are some specific aspects of the deep layered learning system used in

this study that can be good to bear in mind when designing training and validation sets. The representations extracted during training for one supervised learning step is later used (in some shape) as input for the next learning step. As a result, the subsequent model may become over-reliant on the part of the input that comes from the previous supervised step, and not reliant enough on the data that comes from skip-connection from earlier parts of the system. Therefore, if enough data is available or easy to create, a larger pool of training examples can be created than is actually used during each training step. Examples can then be selected randomly with Monte-Carlo sampling for training each learning module. If a large number of instruments or instrument models were used to create the training set, the random sampling can happen on the instrument level. Otherwise, it can happen on the level of the MEs. The validation set can be identical throughout training.

13.5 Deep layered learning

The performance of the system shows that DLL can be used in MIR to build state-of-the-art systems for complex tasks. Deep layered learning draws on many different strategies from machine learning for creating models that generalize well. It is assumed that continuous regions of framewise f_0 s indicate a pitched note. This is a valid assumption by its very definition, and it is used to enforce “validity” according to the definition in Section 3. As a result, the model becomes deeper, as the framewise structure must first be established before computing onsets. How does this affect generalization in relation to end-to-end learning? Take, for example, a system that extracts onsets directly with an RNN.

If the association with framewise f_0 s is not enforced, the system can be expected to focus on, for instance, specific timbral characteristics at onsets whenever that leads to better classification accuracy on the training set. In other words, a system that is not forced to track continuous regions of f_0 s will only do so to the extent that it improves performance on the training set, and instead make other assumptions to untangle the mesh of overlapping partials - for example, assumptions relying on spectral characteristics of the instruments. Systems can always be conceived as relying on a set of assumptions, whether implicitly (through inference) or explicitly (by specification). If the system then is tested on tracks where assumptions of specific timbral characteristics no longer hold, it will fail to generalize to the same extent. A deep model with enforced validity is not as free to infer onsets if no pitch ridge has been established and may therefore perform worse on the training set. However, as the assumption of a pitch ridge is generally valid, this may improve generalization.

Latent representations and skip-connections are used for supplying input data to higher-level learning modules. But if high-level learning modules only rely on data from skip-connections, e.g., connected from the spectrogram, intermediate targets are not enforcing validity, and generalization may suffer. Therefore, the amount of input data provided from skip-connections was somewhat restricted: the deeper representations covered a longer time window, while skip-connections only focused specifically at the onset position. But even when a skip-connection provides input from which overfitting could happen, the representations extracted through more depth will also have been fitted to the characteristics of the training set through intermediate targets. In this roundabout way,

various factors that are hard to understand fully, determine the ability of the system to generalize.

An important concept used in several parts of the system is to use network activations to extract disentangled structures of the data so that invariant processing models can be applied on top of the structures. This includes high-resolution pitch ridges across which onsets can be detected in a tone-shift-invariant way. Tentative notes can also be thoroughly characterized before deciding if they are correct or not. Although these structures represent basic concepts of music, they are not commonly integrated into learning algorithms.

Extracted structures can be very beneficial when expanding the system beyond multiple pitch tracking. The Pitchogram computed by this system (while still under development) was used for state-of-the-art beat tracking (Elowsson, 2016). As another example, it is highly likely that spectral information extracted from the pitch-varying ridge is beneficial for extracting pitched instruments in source separation or for performing pitched instrument recognition.

Acknowledgements

Thanks to Anders Friberg for valuable feedback on the manuscript and Pawel Herman for additional comments.

References

- Alpaydin, E., & Kaynak, C. (1998). Cascading classifiers. *Kybernetika*, 34(4), 369-374.
- Bay, M., Ehmann, A. F., & Downie, J. S. (2009, October). Evaluation of Multiple-F0 Estimation and Tracking Systems. In *ISMIR* (pp. 315-320).
- Benetos, E., & Weyde, T. (2013). Explicit duration hidden markov models for multiple-instrument polyphonic music transcription.
- Benetos, E., & Weyde, T. (2015). An efficient temporally-constrained probabilistic model for multiple-instrument music transcription. 16th International Society for Music Information Retrieval Conference (ISMIR)
- Benetos, E., Cherla, S., & Weyde, T. (2013). An efficient shift-invariant model for polyphonic music transcription. In *6th International Workshop on Machine Learning and Music*.
- Berg-Kirkpatrick, T., Andreas, J., & Klein, D. (2014). Unsupervised transcription of piano music. In *Advances in neural information processing systems* (pp. 1538-1546).
- Bittner, R. M., McFee, B., Salamon, J., Li, P., & Bello, J. P. (2017, October). Deep saliency representations for f0 estimation in polyphonic music. In *Proceedings of the 18th International Society for Music Information Retrieval Conference, Suzhou, China* (pp. 23-27).

- Boogaart, C. G. vd, & Lienhart, R. (2009, June). Note onset detection for the transcription of polyphonic piano music. In *International Conference on Multimedia and Expo (ICME)*, (pp. 446-449). IEEE.
- Böck, S., & Schedl, M. (2012, March). Polyphonic piano note transcription with recurrent neural networks. In *Acoustics, speech and signal processing (ICASSP), 2012 IEEE international conference on* (pp. 121-124). IEEE.
- Böck, S., & Widmer, G. (2013, September). Maximum filter vibrato suppression for onset detection. In Proc. of the 16th Int. Conf. on Digital Audio Effects (DAFx). Maynooth, Ireland (Sept 2013).
- Boulanger-Lewandowski, N., Bengio, Y., & Vincent, P. (2012, June). Modeling temporal dependencies in high-dimensional sequences: application to polyphonic music generation and transcription. In *Proceedings of the 29th International Conference on Machine Learning* (pp. 1881-1888). Omnipress.
- Cheng, T., Mauch, M., Benetos, E., & Dixon, S. (2016, August). An attack/decay model for piano transcription. ISMIR.
- Cont, A. (2006, August). Realtime multiple pitch observation using sparse non-negative constraints. In *International Symposium on Music Information Retrieval (ISMIR)* (pp. 206-211).
- Costantini, G., Todisco, M., Perfetti, R., Basili, R., & Casali, D. (2010, April). Svm based transcription system with short-term memory oriented to polyphonic piano music. In MELECON 2010-2010 15th IEEE Mediterranean Electrotechnical Conference (pp. 196-201). IEEE.
- De Cheveigné, A., & Kawahara, H. (1999). Multiple period estimation and pitch perception model. *Speech Communication*, 27(3-4), 175-185.
- Dressler, K. (2017). Doctoral dissertation.
- Duan, Z., Pardo, B., & Zhang, C. (2010). Multiple fundamental frequency estimation by modeling spectral peaks and non-peak regions. *IEEE Transactions on Audio, Speech, and Language Processing*, 18(8), 2121-2133.
- Elowsson, A. (2018). Deep layered learning in MIR. *Manuscript submitted for publication*, 6 pages.
- Elowsson, A. (2016). Beat Tracking with a Cepstroid Invariant Neural Network. In *17th International Society for Music Information Retrieval Conference (ISMIR)*, (pp. 351-357). International Society for Music Information Retrieval.
- Elowsson, A., & Friberg, A. (2013, July). Modelling perception of speed in music audio. Proceedings of the Sound and Music Computing Conference (SMC).
- Elowsson, A., & Friberg, A. (2017a). Predicting the perception of performed dynamics in music audio with ensemble learning. *The Journal of the Acoustical Society of America*, 141(3), 2224-2242.

- Elowsson, A., & Friberg, A. (2017b). Long-term Average Spectrum in Popular Music and its Relation to the Level of the Percussion. In *Audio Engineering Society Convention 142*, 12 pages. Audio Engineering Society.
- Emiya, V., Badeau, R., & David, B. (2010). Multipitch estimation of piano sounds using a new probabilistic spectral smoothness principle. *IEEE Transactions on Audio, Speech, and Language Processing*, 18(6), 1643-1654.
- FitzGerald, D., Cranitch, M., & Coyle, E. (2005). Generalised prior subspace analysis for polyphonic pitch transcription.
- Friberg, A., Lindeberg, T., Hellwagner, M., Helgason, P., Laís Salomão, G., Elowsson, A., Lemaitre, G., & Ternström, S. (2018). Prediction of three articulatory categories in vocal sound imitations using models for auditory receptive fields. *Journal of the Acoustical Society of America* (in revision).
- Friberg, A., Schoonderwaldt, E., & Juslin, P. N. (2007). CUEx: An algorithm for automatic extraction of expressive tone parameters in music performance from acoustic signals. *Acta acustica united with acustica*, 93(3), 411-420.
- Gao, L., Su, L., Yang, Y. H., & Lee, T. (2017, March). Polyphonic piano note transcription with non-negative matrix factorization of differential spectrogram. In *IEEE International Conference on Acoustics, Speech and Signal Processing (ICASSP)*, (pp. 291-295). IEEE.
- Goldstein, J. L. (1973). An optimum processor theory for the central formation of the pitch of complex tones. *The Journal of the Acoustical Society of America*, 54(6), 1496-1516.
- Goto, M. (2000). A robust predominant-F0 estimation method for real-time detection of melody and bass lines in CD recordings. In *Acoustics, Speech, and Signal Processing, 2000. ICASSP'00. Proceedings. 2000 IEEE International Conference on* (Vol. 2, pp. II757-II760). IEEE.
- Hawthorne, C., Elsen, E., Song, J., Roberts, A., Simon, I., Raffel, C., Engel, J., Oore S., & Eck, D. (2017). Onsets and Frames: Dual-Objective Piano Transcription. arXiv preprint arXiv:1710.11153.
- He, K., Zhang, X., Ren, S., & Sun, J. (2016). Deep residual learning for image recognition. In *Proceedings of the IEEE conference on computer vision and pattern recognition* (pp. 770-778).
- Kalman, B. L., & Kwasny, S. C. (1997). High performance training of feedforward and simple recurrent networks. *Neurocomputing*, 14(1), 63-83.
- Kelz, R., Dorfer, M., Korzeniowski, F., Böck, S., Arzt, A., & Widmer, G. (2016). On the potential of simple framewise approaches to piano transcription. *arXiv preprint arXiv:1612.05153*.
- Kelz, R., & Widmer, G. (2017). An experimental analysis of the entanglement problem in neural-network-based music transcription systems. *arXiv preprint arXiv:1702.00025*.

- Klapuri, A. P. (2003). Multiple fundamental frequency estimation based on harmonicity and spectral smoothness. *IEEE Transactions on Speech and Audio Processing*, 11(6), 804-816.
- Klapuri, A. (2006, October). Multiple Fundamental Frequency Estimation by Summing Harmonic Amplitudes. In *ISMIR* (pp. 216-221).
- Klapuri, A. (2008). Multipitch analysis of polyphonic music and speech signals using an auditory model. *IEEE Transactions on Audio, Speech, and Language Processing*, 16(2), 255-266.
- Krizhevsky, A., Sutskever, I., & Hinton, G. E. (2012). Imagenet classification with deep convolutional neural networks. In *Advances in neural information processing systems* (pp. 1097-1105).
- Maher, R. C., & Beauchamp, J. W. (1994). Fundamental frequency estimation of musical signals using a two-way mismatch procedure. *The Journal of the Acoustical Society of America*, 95(4), 2254-2263.
- Marolt, M. (2001, November). SONIC: Transcription of polyphonic piano music with neural networks. In *Workshop on Current Research Directions in Computer Music* (pp. 217-224).
- Marolt, M. (2004). A connectionist approach to automatic transcription of polyphonic piano music. *IEEE Transactions on Multimedia*, 6(3), 439-449.
- Mauch, M., & Ewert, S. (2013). The audio degradation toolbox and its application to robustness evaluation. In *Proceedings of the International Society for Music Information Retrieval Conference (ISMIR)*.
- Miron, M., Carabias-Orti, J. J., & Janer, J. (2014, October). Audio-to-score Alignment at the Note Level for Orchestral Recordings. In *ISMIR* (pp. 125-130).
- Nakamura, E., Benetos, E., Yoshii, K., Dixon, S. (2018). Towards Complete Polyphonic Music Transcription: Integrating Multi-Pitch Detection and Rhythm Quantization. Proc. 43rd IEEE International Conference on Acoustics, Speech and Signal Processing (ICASSP), 2018.
- Nam, J., Ngiam, J., Lee, H., & Slaney, M. (2011, October). A Classification-Based Polyphonic Piano Transcription Approach Using Learned Feature Representations. In *ISMIR* (pp. 175-180).
- Ng, H. W., Nguyen, V. D., Vonikakis, V., & Winkler, S. (2015, November). Deep learning for emotion recognition on small datasets using transfer learning. In *Proceedings of the 2015 ACM on international conference on multimodal interaction* (pp. 443-449). ACM.
- O'Hanlon, K., Nagano, H., Keriven, N., & Plumbley, M. D. (2016). Non-negative group sparsity with subspace note modelling for polyphonic transcription. *IEEE/ACM Transactions on Audio, Speech and Language Processing (TASLP)*, 24(3), 530-542.

- Pan, S. J., & Yang, Q. (2010). A survey on transfer learning. *IEEE Transactions on knowledge and data engineering*, 22(10), 1345-1359.
- Peeling, P. H., & Godsill, S. J. (2011). Multiple pitch estimation using non-homogeneous Poisson processes. *IEEE Journal of Selected Topics in Signal Processing*, 5(6), 1133-1143.
- Pertusa, A. & Iñesta, J. M. (2008). "Multiple fundamental frequency estimation using Gaussian smoothness," in Proc. IEEE Int. Conf. Acoust., Speech, Signal Process. (ICASSP), pp. 105–108.
- Pesek, M., Leonardis, A., & Marolt, M. (2017). Robust real-time music transcription with a compositional hierarchical model. *PloS one*, 12(1), e0169411.
- Poliner, G. E., & Ellis, D. P. (2006). A discriminative model for polyphonic piano transcription. *EURASIP Journal on Advances in Signal Processing*, 2007(1).
- Raczynski, S., Vincent, E., Bimbot, F., & Sagayama, S. (2010, August). Multiple pitch transcription using DBN-based musicological models. In *2010 Int. Society for Music Information Retrieval Conf.(ISMIR)* (pp. 363-368).
- Ryynänen, M. P., & Klapuri, A. (2005, October). Polyphonic music transcription using note event modeling. In *Applications of Signal Processing to Audio and Acoustics, 2005. IEEE Workshop on* (pp. 319-322). IEEE.
- Schörkhuber, C., Klapuri, A., Holighaus, N., & Dörfler, M. (2014, January). A Matlab toolbox for efficient perfect reconstruction time-frequency transforms with log-frequency resolution. In *Audio Engineering Society Conference: 53rd International Conference: Semantic Audio*. Audio Engineering Society.
- Schramm, R., & Benetos, E. (2017, June). Automatic transcription of a cappella recordings from multiple singers. In *Audio Engineering Society Conference: 2017 AES International Conference on Semantic Audio*. Audio Engineering Society.
- Sethares, W. A., & Staley, T. W. (1999). Periodicity transforms. *IEEE transactions on Signal Processing*, 47(11), 2953-2964.
- Sigtia, S., Benetos, E., & Dixon, S. (2016). An end-to-end neural network for polyphonic piano music transcription. *IEEE/ACM Transactions on Audio, Speech and Language Processing (TASLP)*, 24(5), 927-939.
- Sigtia, S., Benetos, E., Cherla, S., Weyde, T., Garcez, A., & Dixon, S. (2014). RNN-based Music Language Models for Improving Automatic Music Transcription.
- Smaragdis, P., & Brown, J. C. (2003, October). Non-negative matrix factorization for polyphonic music transcription. In *Applications of Signal Processing to Audio and Acoustics, 2003 IEEE Workshop on*. (pp. 177-180). IEEE.
- Srivastava, R. K., Greff, K., & Schmidhuber, J. (2015). Highway networks. *arXiv pre-print arXiv:1505.00387*.

- Sturm, B. L. (2013). Classification accuracy is not enough," *Journal of Intelligent Information Systems*, 41(3), 371-406.
- Su, L., & Yang, Y. H. (2015). Combining spectral and temporal representations for multipitch estimation of polyphonic music. *IEEE/ACM Transactions on Audio, Speech and Language Processing (TASLP)*, 23(10), 1600-1612.
- Thornburg, H. D., & Leistikow, R. J. (2004, May). A new probabilistic spectral pitch estimator: exact and MCMC-approximate strategies. In *International Symposium on Computer Music Modeling and Retrieval* (pp. 41-60). Springer, Berlin, Heidelberg.
- Valero-Mas, J. J., Benetos, E., & Inesta, J. M. (2016). Classification-based Note Tracking for Automatic Music Transcription.
- Valero-Mas, J. J., Benetos, E., & Iñesta, J. M. (2017, June). Assessing the Relevance of Onset Information for Note Tracking in Piano Music Transcription. In *Audio Engineering Society Conference: 2017 AES International Conference on Semantic Audio*. Audio Engineering Society.
- Vincent, E., & Rodet, X. (2004, September). Music transcription with ISA and HMM. In *International Conference on Independent Component Analysis and Signal Separation* (pp. 1197-1204). Springer, Berlin, Heidelberg.
- Vincent, E., Bertin, N., & Badeau, R. (2010). Adaptive harmonic spectral decomposition for multiple pitch estimation. *IEEE Transactions on Audio, Speech, and Language Processing*, 18(3), 528-537.
- Viola, P., & Jones, M. (2001). Rapid object detection using a boosted cascade of simple features. In *Computer Vision and Pattern Recognition, 2001. CVPR 2001. Proceedings of the 2001 IEEE Computer Society Conference on* (Vol. 1, pp. I-I). IEEE.
- Weninger, F., Kirst, C., Schuller, B., & Bungartz, H. J. (2013, May). A discriminative approach to polyphonic piano note transcription using supervised non-negative matrix factorization. In *Acoustics, speech and signal processing (icassp), 2013 IEEE international conference on* (pp. 6-10). IEEE.
- Yeh, C., Robel, A., & Rodet, X. (2005, March). Multiple fundamental frequency estimation of polyphonic music signals. In *Acoustics, Speech, and Signal Processing, 2005. Proceedings. IEEE International Conference* (Vol. 3, pp. iii-225). IEEE.